ORIGINAL ARTICLE



Contrasting physical mechanisms linking stratospheric polar vortex stretching events to cold Eurasia between autumn and late winter

Chuntao Zou^{1,2} · Ruonan Zhang^{3,4} · Pengfei Zhang⁵ · Lei Wang¹ · Ruhua Zhang¹

Received: 12 June 2023 / Accepted: 16 November 2023 / Published online: 30 December 2023 © The Author(s), under exclusive licence to Springer-Verlag GmbH Germany, part of Springer Nature 2023

Abstract

The weak stratospheric polar vortex (SPV) is usually linked to Northern Hemisphere cold spells. Based on the fifth generation of ECMWF atmospheric reanalysis and WACCM model experiments, we use K-means cluster analysis to extract the zonally asymmetric pattern of October-February stratospheric variability, which involves a stretched SPV and hence leads to cold surges in Northern Hemispheric mid-latitudes. There are contrasting effects and mechanisms between autumn (October– November) and late winter (February) SPV stretching events. In October, anomalies in the stratospheric circulation affect the near-surface 16-20 days after the weakening of the SPV. This contributes to a shift in the North Atlantic Oscillation (NAO) towards its negative phase, leading to cold anomalies over northern Eurasia. Together with the weakening of planetary wave-1 during days 31-40, the second stratosphere-troposphere coupling strengthens the East Asian trough and the Siberian high, resulting in Eurasian high-latitude cooling. For November, the suppressed upward propagation of wave-1 during days 11–15 is conducive to anomalous high pressure over northern Europe and thereby European cooling through a stratospheric pathway, while for days 21–30, the weakening of propagating wave-2 over Eastern Europe intensifies the mid-latitude wave train through a tropospheric pathway, favorable for cold temperatures in mid-latitude East Asia. In contrast, the late winter SPV stretching events and the attendant Eurasian coldness during 11-25 days are likely to have been simultaneously driven by the long-lived European high anomaly, which enhanced the upward-propagating tropospheric waves into the stratosphere and thus favored SPV stretching. It indicates that the tropospheric pathway, rather than the stratospheric pathway, plays a dominant role in cold Eurasia following February SPV stretching events.

 $\textbf{Keywords} \ \ \text{Eurasian cold events} \cdot \text{Stratospheric polar vortex stretching} \cdot \text{Stratosphere-troposphere coupling} \cdot \text{Planetary waves}$

- ⊠ Ruonan Zhang rn_zhang@fudan.edu.cn
- Department of Atmospheric and Oceanic Sciences, Institute of Atmospheric Sciences, Fudan University, Shanghai, China
- ² CMA-FDU Joint Laboratory of Marine Meteorology, Shanghai, China
- Shanghai Frontiers Science Center of Atmosphere-Ocean Interaction, Fudan University, Shanghai, China
- ⁴ Key Laboratory of Polar Atmosphere-Ocean-Ice System for Weather and Climate, Ministry of Education, Fudan University, Shanghai, China
- Department of Meteorology and Atmospheric Science, The Pennsylvania State University, University Park, PA, USA

1 Introduction

The stratospheric polar vortex (SPV), one of the important features of large-scale stratospheric circulation, is strongly modulated by vertically upward-propagating tropospheric planetary waves, in turn, can exert influence on the downward propagation of wave activity fluxes and surface changes (Domeisen and Butler 2020; Domeisen et al. 2020; Dunn-Sigouin and Shaw 2015; Garfinkel et al. 2017; Kidston et al. 2015; Sigmond et al. 2013; Scaife et al. 2016; Thompson and Wallace 2001; Waugh et al. 2017; Xie et al. 2020). Previous studies have shown that the stratospheric planetary wave pathway strengthens the linkage between Arctic warming and mid-latitude severe winters (Cohen et al. 2014, 2020). It is well-known that the weak SPV events are often followed by downward migration of the stratospheric northern annular mode (NAM) signals



which are closely related to the negative Arctic Oscillation or North Atlantic Oscillation (AO/NAO) and preceded by anomalous upward wave activity in the upper-troposphere (Baldwin and Dunkerton 1999, 2001; Hitchcock and Simpson 2014; Polvani and Waugh 2004; Wang and Chen 2010; Yang et al. 2016). Numerous studies have quantified the connection between weak SPV events and the intensity of cold air outbreaks (CAOs) in the Northern Hemispheric mid-high latitudes. For instance, compared to strong SPV states, Eurasian CAOs under the weak SPV states feature colder surface air temperature (SAT) over northern Eurasia due to a stronger negative NAO (Huang and Tian 2019). The probability of CAOs over northern Eurasia and the east coast of North America increases by more than 50% within several weeks after the onset of weak SPV events (Kolstad et al. 2010). Huang et al. (2021) found that weak SPV conditions significantly elevate the risk of severe CAOs over midlatitude East Asia and high-latitude Europe, which persists for more than three weeks following weak SPV events. The Alaskan Ridge (AkR) pattern features stratospheric ridge anomalies occupying Eastern Siberia and northern Europe and an anomalous trough occupying Canada, favorable for severe CAOs over North America (Lee et al. 2019). Thus, it is indispensable to have a better understanding of stratosphere-troposphere coupling mechanisms for the weak SPV impacting CAOs for the purpose of improving short-term climate prediction skills.

Typical weak SPV events, such as Sudden stratospheric warming events (SSWs), are defined as complete reversals of the stratospheric westerlies in winter, accompanied by the abrupt rise of Arctic stratospheric air temperature (Baldwin et al. 2021; Butler et al. 2015, 2017; King et al. 2019; Rao et al. 2018, 2019, 2020). SSWs can be catalogued as displacement and split events according to the geometry of the SPV, which is dominated by enhanced upward-propagating planetary wave-1 and wave-2, respectively (Charlton and Polvani 2007; Mitchell et al. 2011, 2013). The timing of the surface response to split events is about a week earlier than that to displacement events, together with colder SAT anomalies over northern Eurasia (Hall et al. 2021; Lehtonen and Karpechko 2016; White et al. 2021). Otherwise, SSWs can be classified into absorbing and reflecting events depending on whether stratospheric planetary waves are reflected back into the troposphere following the onset of SSWs (e.g., Kodera et al. 2008, 2013, 2016; Nath et al. 2014). The northern European-Ural blocking could be a critical precursor to SSWs (Bao et al. 2017; Martius et al. 2009; Woollings et al. 2010), which strengthens the climatological wave-1 or wave-2 component before the onset of SSWs (Garfinkel et al. 2010; Huang et al. 2018; Lu et al. 2021). Except for the stratospheric pathway, atmospheric blockings can directly trigger tropospheric circulation changes and then continental CAOs. Other studies suggest that the CAOs in East Asia prior to SSWs are solely owing to instantaneous upstream Ural blocking development rather than downward-propagating stratospheric signals (e.g., Kolstad et al. 2010; Lu et al. 2021; Luo et al. 2016).

In addition to SSWs, other weak SPV patterns can be identified by using cluster analysis. For instance, selforganizing maps are applied to wintertime mid-tropospheric height anomalies to obtain a Western Hemisphere circulation pattern favorable for the displacement of the SPV to North America through enhanced (suppressed) wave-2 (wave-1) component entering the stratosphere (Tan and Bao 2020). Kretschmer et al. (2018b) performed a hierarchical cluster analysis on the January and February geopotential height anomalies at 100 hPa to capture the symmetric and asymmetric modes of weak SPV states and contrasted their difference in the dynamical mechanisms. The zonally symmetric mode, which resembles absorbing SSWs, is associated with the negative NAO and cooling over northern Eurasia, while the zonally asymmetric mode is associated with planetary wave reflection over Canada and hence robust cooling over North America. Based on this study, Cohen et al. (2021) mainly focused on a zonally asymmetric pattern (so-called SPV stretching events) and its tropospheric impacts from October through December by adopting K-means cluster analysis. The frequency of zonally symmetric and asymmetric modes increases significantly during both autumn and winter (Cohen et al. 2021; Kretschmer et al. 2018b; Liang et al. 2023). The increasing frequency of weak SPV states can account for nearly 60% of the cooling region over midlatitude Eurasia; this proportion rises to about 80% when El Niño-Southern Oscillation variability is included, indicating that persistent weak SPV and tropical variability together contribute to Eurasian cooling (Kretschmer et al. 2018a). Besides the SPV stretching events, an empirical orthogonal function method is applied to extract the planetary wave-1 pattern associated with stratospheric variability, which features a high surface pressure anomaly over Alaska and a low anomaly over eastern North America, thus favoring cold surges over North America via stratosphere–troposphere interactions (Ding et al. 2022, 2023).

With the increasing importance of weak SPV, most existing literature appears to emphasize the crucial role of SSWs in Eurasian and North American coldness (e.g., Hall et al. 2021; Kodera et al. 2016; Xu et al. 2022; Zhang et al. 2020), the SPV stretching events and related surface responses are only marginally mentioned in several studies (Cohen et al. 2021, 2022; Ding et al. 2022, 2023; Kretschmer et al. 2018b; Liang et al. 2023; Matthias and Kretschmer 2020; Messori et al. 2022; Shen et al. 2023). However, the occurrence probability of SSWs is less than that of SPV stretching events (Cohen et al. 2021; Liang et al. 2023). In addition, although the SSW in January 2021 may contribute to cold spells over Texas (Lu et al. 2021; Zhang et al. 2022), the contribution



of the SPV stretching in February 2021 to the Texas CAOs is greater than the SSW in January 2021 (Cohen et al. 2021). Therefore, there is an urgent need to better understand the possible effects of SPV stretching events. In contrast to those previous studies that have illustrated the relationship between the autumn and winter SPV stretching events and surface cold spells in North America on the seasonal timescales, this study aims to investigate the sub-seasonal characteristics of SPV stretching events occurring in autumn and winter, as well as the underlying linkage between SPV stretching and Eurasian cooling. The paper is organized as follows: Sect. 2 describes the data and methods. Section 3 discusses the main characteristics of monthly SPV stretching events and the underlying physical mechanisms that influence cold SAT anomalies over Eurasia. Section 4 provides the main conclusions of this paper.

2 Data and methods

In this work, we use the four-time-daily mean datasets from the fifth generation of ECMWF atmospheric reanalysis (ERA5; Hersbach et al. 2020), with $1^{\circ} \times 1^{\circ}$ horizontal resolution and 13 pressure levels from 1000 to 10 hPa. The variables include geopotential height, air temperature, zonal and meridional wind at pressure levels, sea level pressure (SLP), and SAT. These variables are calculated from September to April 1980–2021. A high-top model, the Whole Atmosphere Community Climate Model (WACCM) version 4, is used to examine the surface impacts of the SPV stretching events. This model configuration has 1.98° × 2.58° horizontal resolution and 66 vertical levels with the lid of the model at 5×10^{-6} hPa (Smith et al. 2014). The control experiment with prescribed surface conditions from 1980 to 2010 is conducted to facilitate contrast with observation, which is integrated for 210 years, with the first 10 years discarded for model spin-up. We define the SAT index for high-latitude Eurasia and mid-latitude East Asia as the area-weighted average of SAT anomalies over the region of 45°-125° E, $45^{\circ}-60^{\circ}$ N and $80^{\circ}-125^{\circ}$ E, $30^{\circ}-45^{\circ}$ N, respectively. Moreover, three key domains with significant anomalies in the 100 hPa wave activity flux (WAFz) are selected to detect the characteristics of wave reflection following SPV stretching events: Siberia (90°–135° E, 50°–70° N), Eastern Europe $(20^{\circ}-55^{\circ} \text{ E}, 45^{\circ}-65^{\circ} \text{ N})$, and $\text{Europe}(0^{\circ}-40^{\circ} \text{ E}, 45^{\circ}-75^{\circ}$ N). The lower stratosphere (100 hPa) is chosen in this study to demonstrate the importance of stratosphere-troposphere coupling (Cohen et al. 2021; Huang et al. 2021; Kretschmer et al. 2018b). Anomalies are calculated by subtracting the daily climatological mean values from 1980 to 2021.

K-means cluster analysis, an unsupervised clustering algorithm, is used to analyze daily geopotential height anomalies at 100 hPa during the autumn and winter months

(October-February) spanning from 1980 to 2021, encompassing a total of 6191 days, to pinpoint the SPV stretching events. The goal of K-means clustering is to minimize the Euclidean distance of n observations from k-cluster centroids. Following Cohen et al. (2021) and Kretschmer et al. (2018b), we obtain 5 clusters (P1-P5) from stronger to weaker SPV states, and the P4 pattern, representative of a stretched SPV, is the focus of our study. The probability of P4 occurrence in this study is 24.8% (Fig. 1), similar to that (23.6%) in Cohen et al. (2021). To explore the possible surface impacts of the P4 pattern on the sub-seasonal timescales, the ONDJF (October–February) P4 pattern (Fig. 2a) is split up into five individuals (Fig. 2b-f) as monthly P4 patterns that differ from Cohen et al. (2021). Cohen et al. (2021) defined SPV stretching events as one or more consecutive P4 days, whereas this study projects the daily geopotential height anomalies at 100 hPa onto the monthly P4 pattern to calculate standardized daily P4 index, and the persistent P4 event is identified when the standardized value exceeds 0.5 for at least 5 consecutive days or the value exceeds 1 at least 3 consecutive days in observations following the method used in Tan and Bao (2020). We then calculate the value of the spatial correlation coefficients between observed P4 pattern (Fig. 2a) and simulated daily geopotential height anomalies and similar P4 patterns (Fig. 2g-1) are obtained when correlation coefficients exceed 0.4 and are sustained for more than 4 days in simulations. The first day greater than this threshold value is defined as the central day (day 0) for a persistent event (i.e., the day 0 denotes the start day with P4 index exceeding 0.5 or 1 in observations and correlation coefficients exceeding 0.4 in simulations).

In order to diagnose the propagation of planetary waves in quasi-geostrophic spherical coordinates, the Eliassen–Palm (EP) flux and three-dimensional WAF (Plumb 1985) are calculated in this study according to the expression of Andrews et al. (1987) and Wang and Yasunari (1994). We also apply the Fourier transformation to the latitude circle to gain the zonal wave-1 and wave-2 components of geopotential height, EP flux, and eddy heat flux (e.g., Lu et al. 2021; Tan and Bao 2020).

3 Results

3.1 Classification of autumn and winter SPV based on cluster analysis

Figure 1 shows the five clusters of 100 hPa geopotential height anomalies from October to February to capture SPV variability in observations. The P1 and P2 clusters represent the stronger SPV states and show a decreasing trend in frequency, whereas both P4 and P5 show the weaker SPV states and an increasing trend in frequency. Cluster 3 (P3),



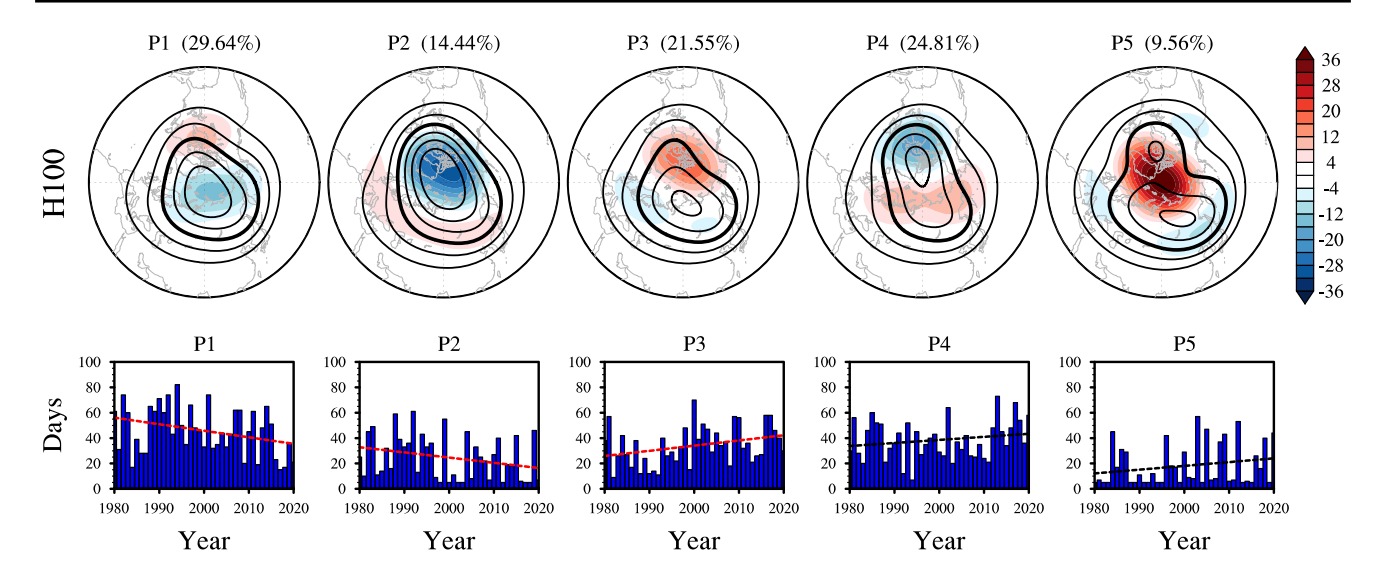


Fig. 1 The K-mean cluster of 100-hPa geopotential height [10 geopotential meters (dagpm)] anomalies in autumn and winter (ONDJF) from 1980 to 2021 in observations. Composites of 100-hPa geopotential height (contour; contour interval is 20 dagpm; 1580 dagpm contour is bolded) and its anomalies (color shading; units: dagpm) for all days assigned to P1-P5 (upper row). Percentage of occupation

frequency assigned to the same cluster is indicated in parentheses. Yearly frequency for P1–P5 pattern days (blue bars), with dashed lines exhibiting linear trend (lower row). The dashed red lines denote statistically significant negative (positive) trend at the 90% confidence level

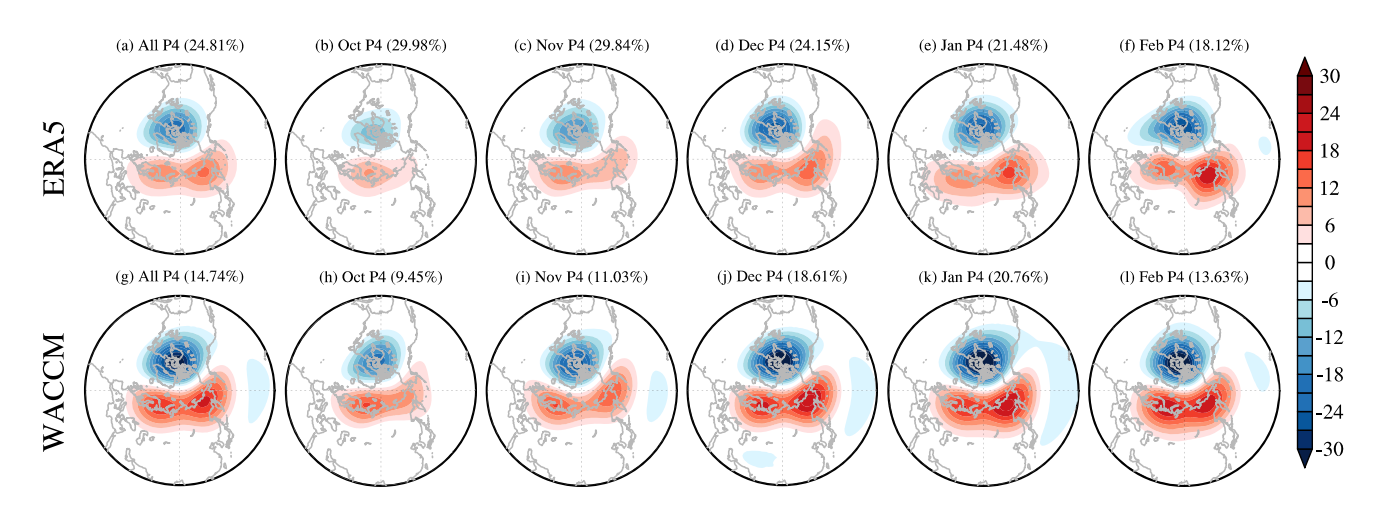


Fig. 2 Same as Fig. 1, but for autumn—winter (ONDJF) and monthly SPV stretching events (P4) pattern in observations (a–f) and WACCM control runs (g–l)

acquiring little attention in case studies, presents a displaced SPV. Contrasting the two weak SPV patterns (P4 vs P5), P5 represents a disturbed SPV and is characterized by zonally symmetric positive height anomalies in the lower stratosphere over the polar region (the SSW-like mode), while P4 shows a stretched SPV and features zonally asymmetric height anomalies in the lower stratosphere with distinct positive anomalies over northern Eurasia and negative anomalies over Canada. These findings are generally consistent with Cohen et al. (2021), who investigated the first five clusters of SPV from October-December, but with a slight difference in the spatial pattern and the percentage of each cluster.

Approximately 25% of autumn and winter days are allocated for P4, while 10% or so are assigned to P5, suggesting the increasingly frequent occurrence of P4 and associated implications in surface impacts. When we consider the five clusters in the WACCM experiment, a similar P4 (Fig. 2g) and P5 (figure not shown) pattern is simulated, with a frequency of approximately 15% and 12%, respectively. It is worth noting the transition from one positive height anomaly centered near Barents-Kara Seas in autumn P4 (Fig. 2b, c, h, i) to two centers of ridge anomalies anchored over Eastern Siberia and Barents-Kara Seas in winter P4 (Fig. 2d–f, j–l). Due to the lack of research and the overwhelmingly higher



proportion of P4 than those of P5, the present study will focus on P4 (SPV stretching events).

To assess the delayed surface impacts over Eurasia in more detail, we next plot the temporal evolution of Eurasian SAT anomaly in observations and model experiments from day - 10 to day 40 for SPV stretching events occurring in October, November and February (Fig. 3a-f). In general, there are different locations and timing of surface cooling on the sub-seasonal timescales. For SPV stretching events that onset in October (Fig. 3a, d), cold anomalies occur over high-latitude Eurasia during days 21–25 and 36–40, with the latter being more pronounced. A similar surface cooling over Eurasian high-latitudes can be detected in model experiments, but with prominent cold anomalies during days 6-15 and 36-40. However, it is hard to discover evident cold temperatures over mid-latitude East Asia in observations and simulations. For November SPV stretching events (Fig. 3b, e), both high-latitude Eurasia and mid-latitude East Asia experienced noticeable cooling. We find evident cooling over high-latitude Eurasia in the following 20 days after SPV stretching and over mid-latitude East Asia during days 20-30, which is well reproduced in model experiments except for 5 days in advance (days 15-25). For February SPV stretching events, significant cold temperatures over Eurasian high-latitudes appear during days 5–26 in experiments (Fig. 3f), resembling the observations that cooling occurs during days 12-30 (Fig. 3c). For December and January, most of previous studies mainly focused on SSWs because these months show the larger stratospheric variability compared to October and November (e.g., Lu et al. 2021; Rao et al. 2020; Xu et al. 2022). Unlike the SSWs that occurred in December and January followed by robust Eurasian cooling, the SPV stretching events during these months feature the absence of cold Eurasia (figure not shown). Therefore, the December-January SPV stretching events are not discussed in the present study due to the lack of significantly and continuously delayed surface impacts over Eurasia. It is found that the magnitude of surface cooling that occurred following February

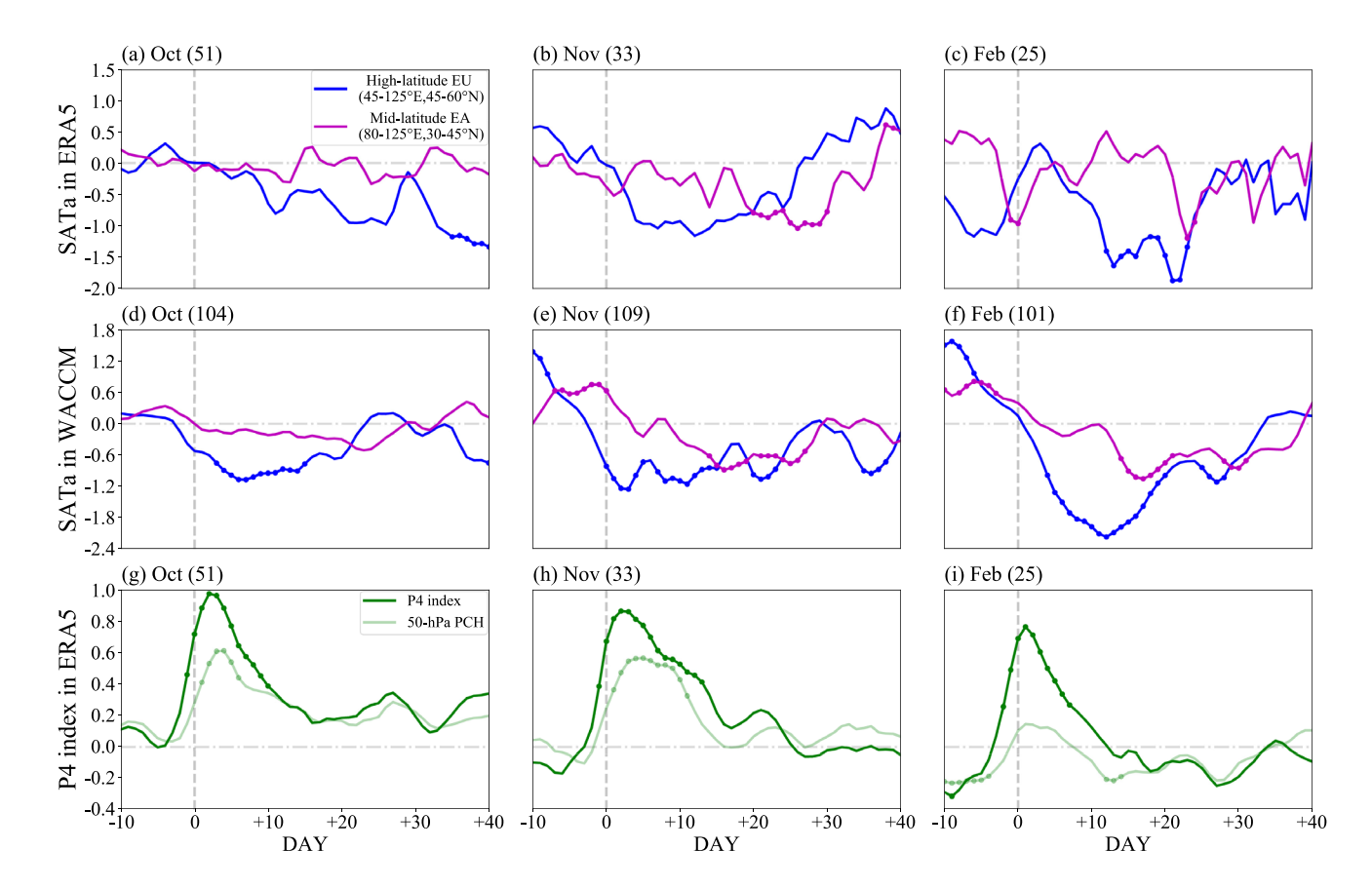


Fig. 3 a–c Time evolution of area-averaged daily surface air temperature (SAT; units: K) anomalies over Eurasian high-latitudes (45°–125°E, 45°–60°N; blue lines) and mid-latitudes (80°–125° E, 30°–45° N; purple lines) during days – 10 to 40 following SPV stretching events that occurred in autumn and late winter in observation. **d–f** Same as **a–c** but for the simulation. **g–i** Same as **a–c** but for

the normalized P4 index at 100-hPa (green lines) as well as the polar cap height (PCH; 65–90° N) index at 50-hPa (light green lines). The normalized PCH index at 50-hPa averaged over 0–100° E (0–180° E) in **g–h** (i). The dots denote that the SAT anomaly is significant to their climatology at the 90% confidence level. The sample sizes for the composite analysis are shown in the brackets



SPV stretching events is stronger than that in October and November, which is potentially related to more robust SPV stretching in February than in October and November (Fig. 2). In order to examine the linkage between the magnitude of the SPV stretching pattern and surface signal, the daily normalized P4 index at 100 hPa and the polar cap height (PCH) index at 50 hPa (Fig. 3g-i) are calculated based on the approach similar to that used by Kretschmer et al. (2018b). The relatively short duration (12 days) of significantly high P4 values for autumn and late winter P4 events is generally consistent with Kretschmer et al. (2018b). It is apparent that both the P4 and PCH indices are significant within the 10 days after the detection of autumn events (Fig. 3g-h), which indicates that the autumn weak polar vortex signals emerge in the lower stratosphere. While for late winter (Fig. 3i), the associated signals are insignificant at 50 hPa and only significant at the atmospheric levels below 100 hPa. Therefore, in the absence of deepened stratospheric signals and related downward propagation, the surface cooling over Eurasian high-latitudes following the late winter events is mainly due to tropospheric processes (Fig. 3c, i), indicative of irrelevant linkage between the magnitude of the stratospheric pattern and surface impacts.

3.2 Mechanisms associated with autumn SPV stretching events

How can autumn SPV stretching events influence the SAT over Eurasia with a lead time of several weeks? To answer this question, we examine the temporal evolution of the normalized PCH anomaly. This metric is one of the most effective for diagnosing the downward propagation of stratospheric signals during the duration of weak SPV events. It can serve as an alternative to the NAM index; positive (negative) PCH anomalies correspond to negative (positive) NAM anomalies (Baldwin and Thompson 2009; Kim et al. 2014; Peings and Magnusdottir 2014; Sun et al. 2015; Rao et al. 2020). Pressure-temporal evolutions of the normalized PCH anomalies from days – 10 to 40 for autumn and late winter SPV stretching events are shown in Fig. 4. Distinct characteristics can be seen in the vertical propagations of circulation anomalies associated with SPV stretching events that occurred in October, November, and February. We first investigate the SPV stretching events in autumn.

The autumn SPV stretching events are characterized by conspicuous positive PCH anomalies throughout the stratosphere and troposphere over Eurasia from days 0–10, with the positive anomalies centered at the lower stratosphere (50 hPa) that extend to the troposphere (Fig. 4a, b).

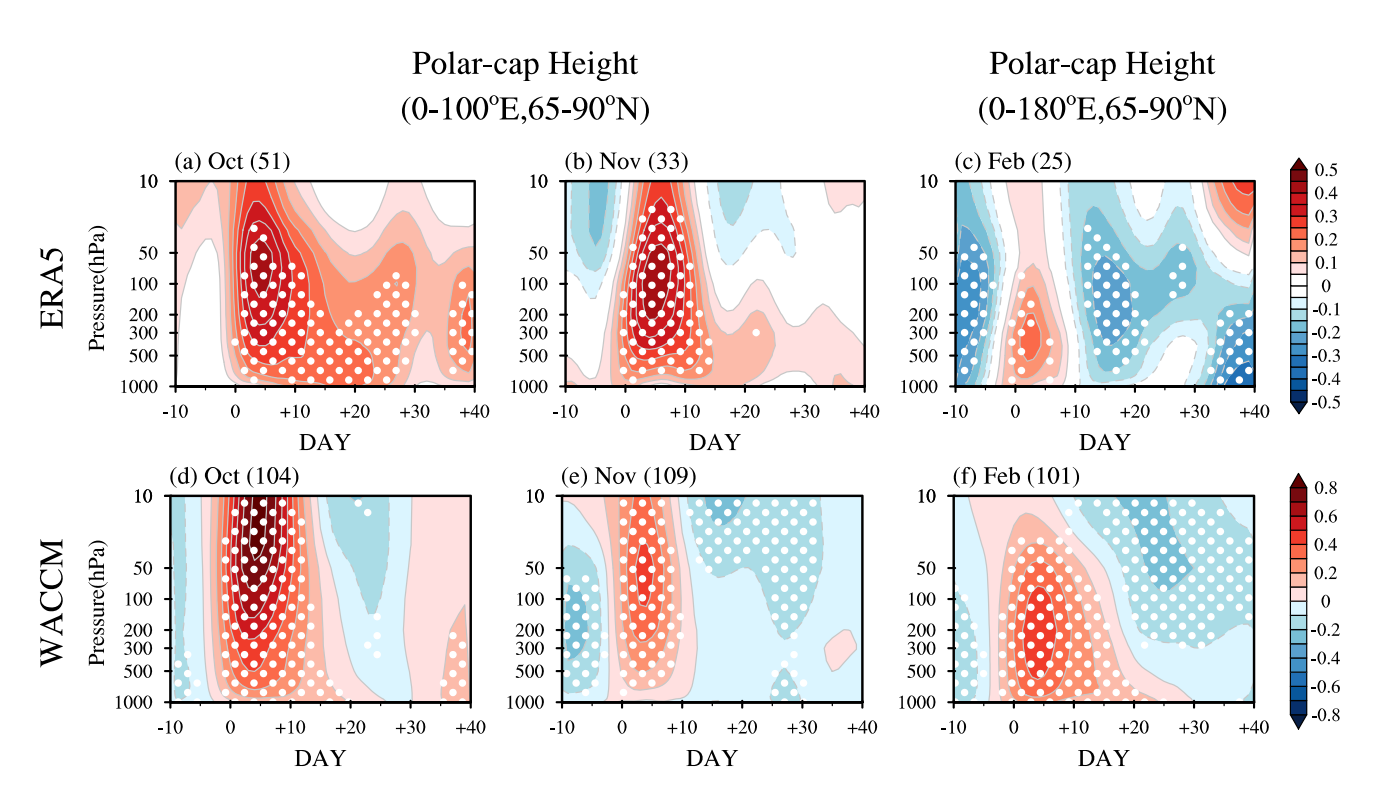


Fig. 4 a–b Time evolution of normalized daily polar cap height (PCH; 65–90° N) anomalies averaged over 0–100° E for October and November SPV stretching events in observations. **c** Same as **a–b** but averaged over 0–180° E for the February SPV stretching events. **d–f**

Same as **a-c** but for WACCM experiments. The PCH anomalies are smoothed by 7-day running average. White stippling indicates statistical significance at the 90% confidence level



Analogous results can be found in model experiments; robust positive PCH anomalies extend from the upper stratosphere to the surface through days 0–10 after SPV stretching events (Fig. 4d, e). These consistent vertical positive PCH anomalies serve as indicators of robust stratosphere-troposphere interactions. Following the onset of October SPV stretching events, the positive PCH anomalies extend downward to the lower-troposphere and near-surface, at a maximum during days 16–20. Subsequently, positive PCH anomalies migrate upward from the troposphere into the lower stratosphere during days 21-30 and then extend downward into the midtroposphere during days 36-40, possibly reflecting a second strong coupling of stratosphere and troposphere (Fig. 4a). The first stratosphere–troposphere interaction sets a favorable condition in the troposphere for a second weak coupling during days 36-40, which occurs without significant SPV stretching features (Fig. 3g). Comparing the WACCM simulation with ERA5, the delayed effects in October SPV stretching events are weaker during days 10-20, as is the absence of the second stratosphere-troposphere coupling during days 31-40 (Fig. 4d). Unlike October SPV stretching events, the positive PCH anomalies following November SPV stretching events emerge in the lower-stratosphere and the troposphere during days 0-10, featuring a weaker propagation (Fig. 4b).

Considering the prolonged delayed surface impacts of monthly SPV stretching events, another question that needs to be addressed is the potential overlap between October events and November events. Specifically, whether the first coupling of the November events was miscounted as the second coupling of the October events? An interval of 30 days between two events (day 0–day 0) is employed to ensure there is no overlap between the two events. Figure 5 shows the lifetime (ERA5 reanalysis) and the probability for overlapping impacts (both ERA5 reanalysis and WACCM simulations) of October and November SPV stretching samples. For ERA5 reanalysis,

reanalysis and WACCM
November SPV stretching

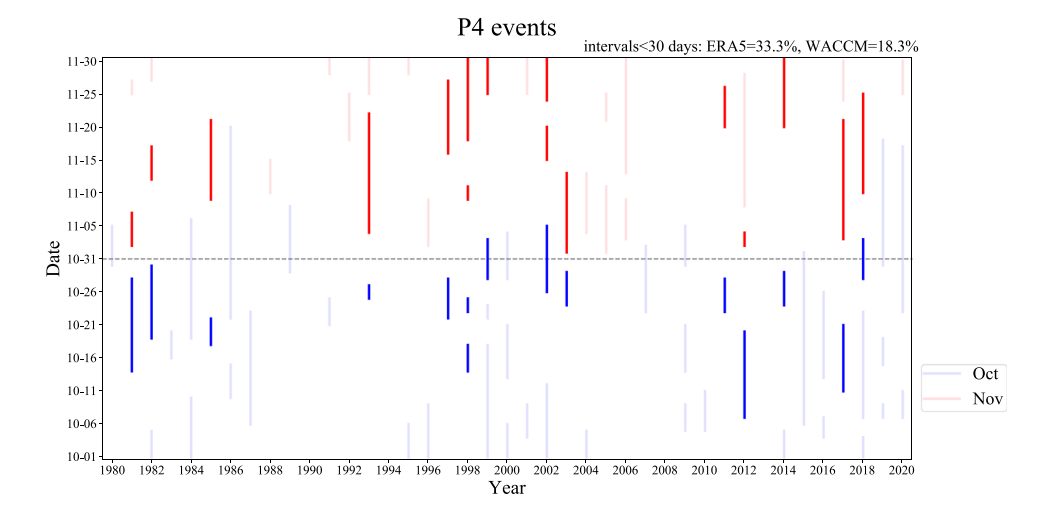
Fig. 5 The distribution and lifetime of individual SPV stretching events in October and November in observations. The deep colour bars present two

events within the intervals of

30 days

there are 17 events with an interval of less than 30 days identified out of the 51 October SPV stretching events. For WACCM simulations, 19 consecutive events are identified by analyzing 104 October SPV stretching events (figure not shown). The probability of the overlap between October and November P4 under October P4 emerging conditions is relatively low in observations (33.3%) and model experiments (18.3%). We also find that the second coupling of October events remains significant in the presence of the removal of the overlapping events with an interval of less than 30 and 40 days (figure not shown). Therefore, we will focus on the autumn and late winter surface impacts of SPV stretching events without the need to consider the potential overlapping effects.

In order to reveal the stratospheric mechanisms associated with autumn surface impacts of SPV stretching events, the pentad evolution of atmospheric anomalies following October SPV stretching events in observation and simulation is shown in Figs. 6, 7. Over the composite SLP map, there is a high-pressure anomaly over the Gulf of Alaska from days -5 to -1, which can also be found in Cohen et al. (2021), leading to a noticeable North American cooling from days -5 to 5 (Fig. 6b, c). The downward extension of stratospheric PCH anomalies gives rise to the transition from relatively low pressure to high pressure centered near Greenland during days 0–20, corresponding to a negative NAO-like pattern (Fig. 6c-f). The 500 hPa geopotential height anomalies reveal a similar pattern to the SLP anomalies, with anomalous high developing over the Arctic-North Eurasian region, reflecting a vertically barotropic structure (Fig. 6l-p; Fig. 7d, e). The cold anomalies over northern Eurasia first emerge during days 16–25 (Fig. 6f, g), while the modeled cooling is more robust during days 6–15 (Fig. 7a, b). After day 30, the Siberian high strengthened gradually, and the strong cold anomalies developed again over highlatitude Eurasia (Fig. 6g-j; Fig. 7c). Likewise, the midtropospheric ridge anomalies in Arctic-Europe and trough





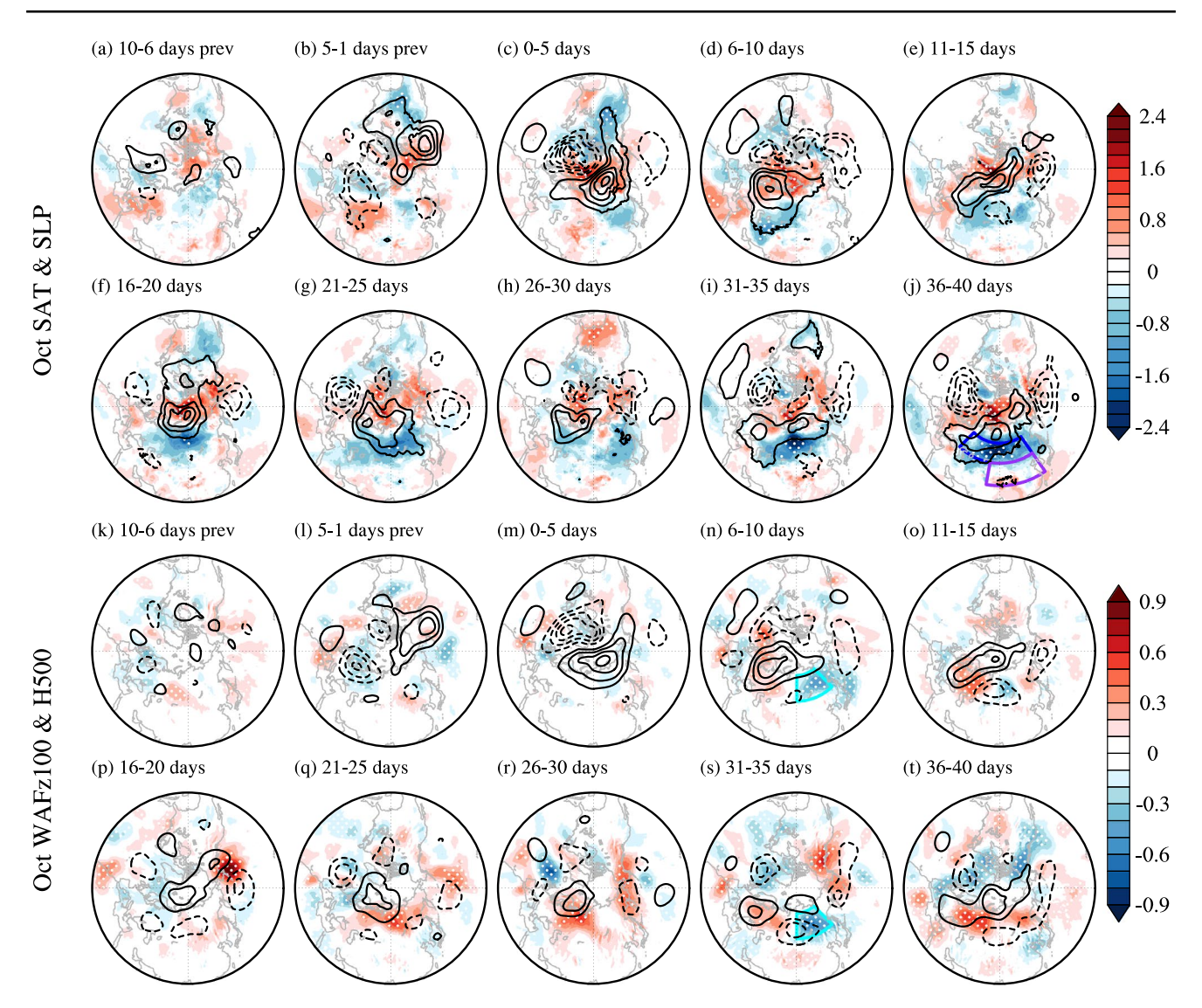


Fig. 6 a–j Spatial pattern of SAT (color shading; units: K) and sea level pressure (SLP; contour; contour interval is 1 hPa) anomalies during days – 10 to 40 for October SPV stretching events in observations. White stippling denotes statistical significance for SAT at the 90% confidence level. Solid (dashed) contours denote positive (negative) values, and zero contours are omitted. The blue and pur-

ple boxes in **j** represent the region of high-latitude Eurasia and midlatitude East Asia, respectively. **k-t** Same as **a-j** but for vertical wave activity flux at 100-hPa (color shading; $0.01 \text{ m}^2 \text{ s}^{-2}$) and geopotential height anomalies at 500-hPa (contour; contour interval is 1.5 dagpm). Cyan boxes in **n** and **s** highlight the key region of anomalous downward propagation of planetary waves

anomalies in Central Siberia-East Asia occur during days 31–40 (Fig. 6s–t; Fig. 7f).

To further investigate the underlying mechanisms of the stratosphere–troposphere interactions, we analyzed the vertical component of the 100 hPa wave activity flux (WAFz100), as the 100 hPa is a useful indicator of the stratosphere–troposphere coupling. Negative WAFz100 anomalies are found over Siberia during the first cold event (days 0–15), suggesting significantly anomalous downward propagation of stratospheric wave activity fluxes into the troposphere (Fig. 6m–o; Fig. 7d), as a similar feature is seen in the PCH anomaly (Fig. 4a, d). For the second cold event, positive WAFz100 anomalies over Siberia during

days 21–30 indicate enhanced upward-propagating planetary waves (Fig. 6q, r) and then depressed waves in the following days in both observation and simulation (Fig. 6s, t; Fig. 7f), in agreement with the upward and downward extension of PCH anomalies (Fig. 4a). It can be found that the negative wave-activity anomalies over Central Siberia appear during days 6–10 for both observation and simulation and days 31–35 for observation (days 36–40 for simulation) separately. The combination of a strengthened Siberian high and an anomalously deepened trough located in East Asia related to the stratosphere–troposphere coupling is favorable for cold anomalies over high-latitude Eurasia through days 31–40.



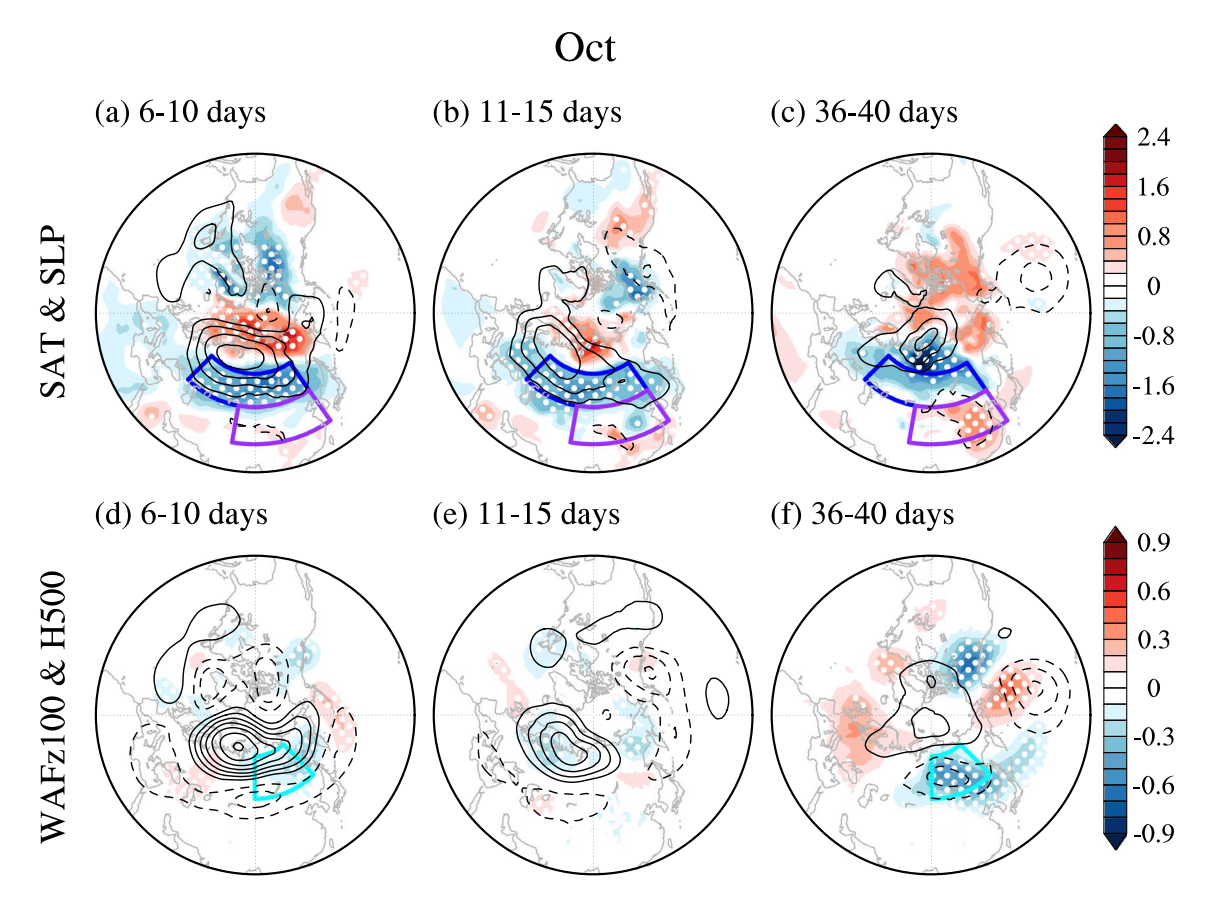


Fig. 7 As in Fig. 6, but for WACCM experiments. The intervals of 500-hPa geopotential height anomalies are 1 dagpm

To separate the relative contributions of planetary waves 1 and 2, the related eddy heat flux anomalies between 45° and 75° N are further diagnosed, as it is approximately proportional to the vertical component of the EP flux (Andrews et al. 1987). Figure 8 shows the eddy heat flux anomalies during days – 10 to 40 of SPV stretching events, and Fig. 9 shows the EP flux anomalies for total waves, wave-1 and wave-2 components. For October events, upward propagation of planetary wave-1 at 100 hPa is suppressed through days - 5 to 10 in both observation and simulation (Fig. 8a, d), while the depression at 300 hPa occurs three days before that at 100 hPa (Fig. 8b), generally consistent with the negative WAFz100 anomalies averaged over the Siberia (Fig. 8c). It should be noted that the simulated wave-1 during the first cold event is stronger in magnitude and longer in duration than observed. For the second cold event, the negative anomalies of wave-1 eddy heat flux at 100 hPa appear during days 28-32 in simulation, slightly earlier than the observation occurring during days 35-40. It can be inferred that for the October SPV stretching events, the planetary wave-1, generally opposite to planetary wave-2, plays an important role in the stratosphere-troposphere interactions and associated surface cold surges. This conclusion is further demonstrated by the following analysis

of wave-1 component anomalies of the EP flux (Fig. 9a-d). It can be seen that the upward propagation of the wave-1 component is suppressed (strengthened) in the mid-latitude (high-latitude) stratosphere during days 0–5 and gradually recovers in the following pentad (Fig. 9a, b). In contrast, the anomalous downward propagation of the wave-1 component moved northwards to about 60°N during the second cold event (Fig. 9c, d), as seen in the WAFz100 map (Fig. 6s). Figure 10 shows the linear interference between wave-1 geopotential height anomalies at 100 hPa and the corresponding climatological components. During days 0-5, the spatial pattern of the wave-1 geopotential height anomalies is outof-phase with that of the climatology (Fig. 10a), indicating a destructive interference between them and hence fewer tropospheric waves propagating upward into the stratosphere (Smith and Kushner 2012). Although days 6–10 also show a destructive interference between the wave-1 component of geopotential height anomaly and climatology, the center of positive anomaly has a westward shift of about 90 degrees, reducing the depression of the upward propagation as days 0-5 (Fig. 10b). There is a constructive interference during days 31-35 and again a destructive interference during days 36-40, manifesting more upward-propagating wave-1 components and then fewer waves, respectively (Fig. 10c, d).



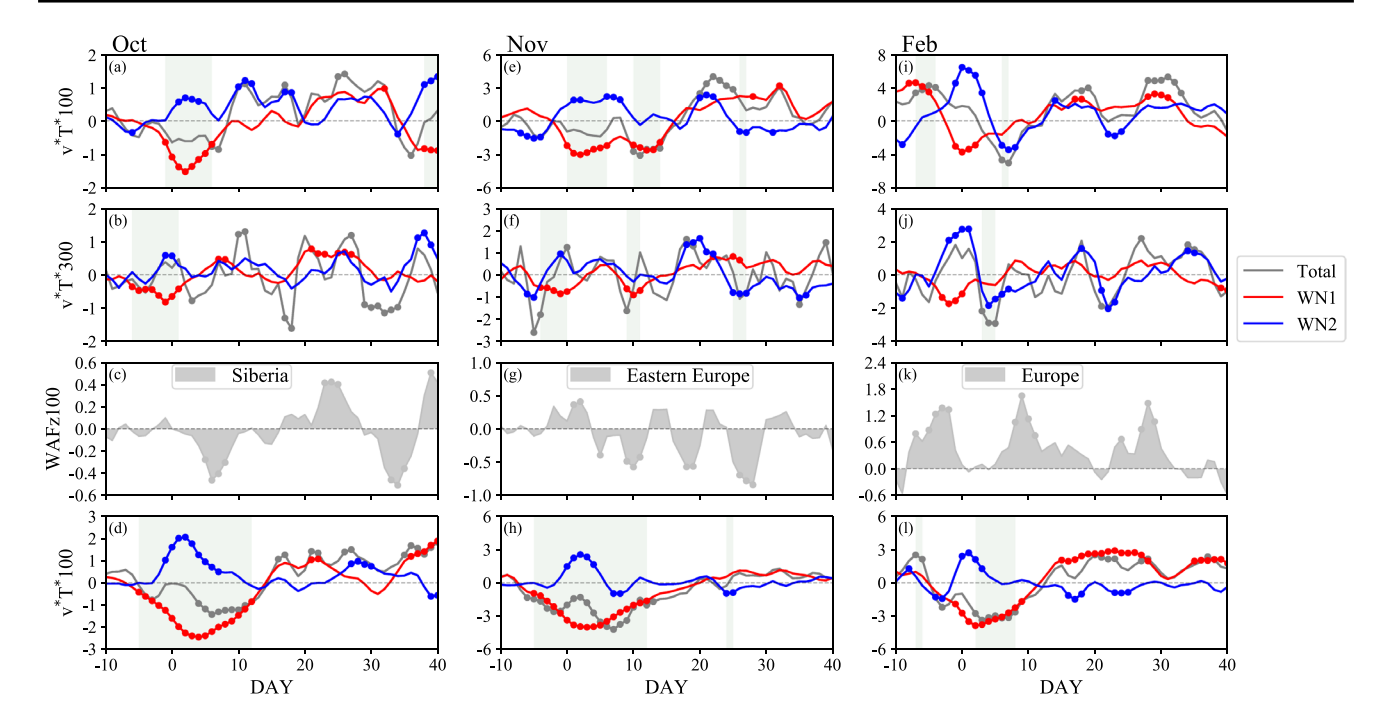


Fig. 8 a–d Composite anomalies of observed a 100-hPa and b 300-hPa eddy heat flux averaged over 45–75° N, c 100-hPa vertical wave activity flux area-averaged over Siberia (90°–135° E, 50°–70° N), and d simulated 100-hPa eddy heat flux averaged over 45–75° N for October SPV stretching events. The gray lines denote total waves of eddy heat flux, and the red (blue) lines denote wave-1 (wave-2). The light green bars in a–h (i–l) highlight the significantly weakened

upward propagation of wave-1 or wave-2 (strengthened or weakened upward propagation of total waves). The dots indicate statistically significant anomalies at the 90% confidence level. **e-h** and **i-l** Same as **a-d** but for November and February SPV stretching events. **g** and **k** Same as **c** but area-averaged over Eastern Europe $(20^{\circ}-55^{\circ} \text{ E}, 45^{\circ}-65^{\circ} \text{ N})$ and Europe $(0^{\circ}-40^{\circ} \text{ E}, 45^{\circ}-75^{\circ} \text{ N})$

These results of linear interference are generally consistent with the vertical propagation of WAF and EP fluxes, as in Figs. 8, 9.

Analogue to October, the observed and simulated atmospheric circulation anomalies for November SPV stretching events are shown in Figs. 11, 12, respectively. We still find two cold episodes, one in Europe and the other in East Asia. During days -5 to 15, an anomalous high ridge migrates from Alaska to northwestern Eurasia, corresponding to the migration of prominent surface cooling from North America to high-latitude Eurasia (Figs. 11b-d, l-n, 12a, e). Subsequently, the spatial pattern of SLP and 500 hPa geopotential height reveals a wave train structure over the mid-latitudes. Specifically, the high pressure over northwestern Eurasia moves southeastward (Fig. 11e-h), and the Ural ridge and the East Asian trough enhance gradually (Fig. 11p-r), leading to cold anomalies in East Asia during days 16-30 (Fig. 11g-h). The simulation can generally reproduce the development of anomalous ridge and Eurasian cold surges; however, the peak of mid-latitude cold surges is during days 16-25 (Fig. 12b-d, f-h). Although the PCH plot shows a robust stratosphere-troposphere interaction (Fig. 4b, e), we still find intermittent anomalous downward-propagating planetary waves near Eastern Europe during days 6-30 (Figs. 8g, 11n-r), which is responsible for the cooling over Europe and then East Asia. For simulation, the location of anomalous downward-propagating planetary waves is slightly shifted eastward to Western Siberia compared to observations (Fig. 12f, g).

Figure 8e-h shows eddy heat flux anomalies associated with planetary wave-1 and wave-2 for November SPV stretching events. For the high-latitude coldness, there is significantly weakened upward propagation of wave-1 at 100 hPa (300 hPa) during days 0-14 (days - 4 to 11), while in simulation, the suppression lasts from days - 5 to 12. A similar net depression of wave-1 propagation can be found in the EP fluxes and the 100-hPa geopotential height during days 0-10 (Figs. 9e, f, 10e, f), suggestive of a predominant role of wave-1 in the development of European cold event. For the mid-latitude coldness, negative eddy heat flux anomalies are found in the wave-2 component during days 25-30 at both 100 hPa and 300 hPa. It is evident that the upward propagation of wave-2 components is suppressed in the mid-high latitude stratosphere during days 26-30, accompanied by anomalous EP-flux divergence in the stratosphere (Fig. 9h) and the destructive interference between anomalous and climatological 100 hPa geopotential height (Fig. 10h). The wave activities during days 26~30



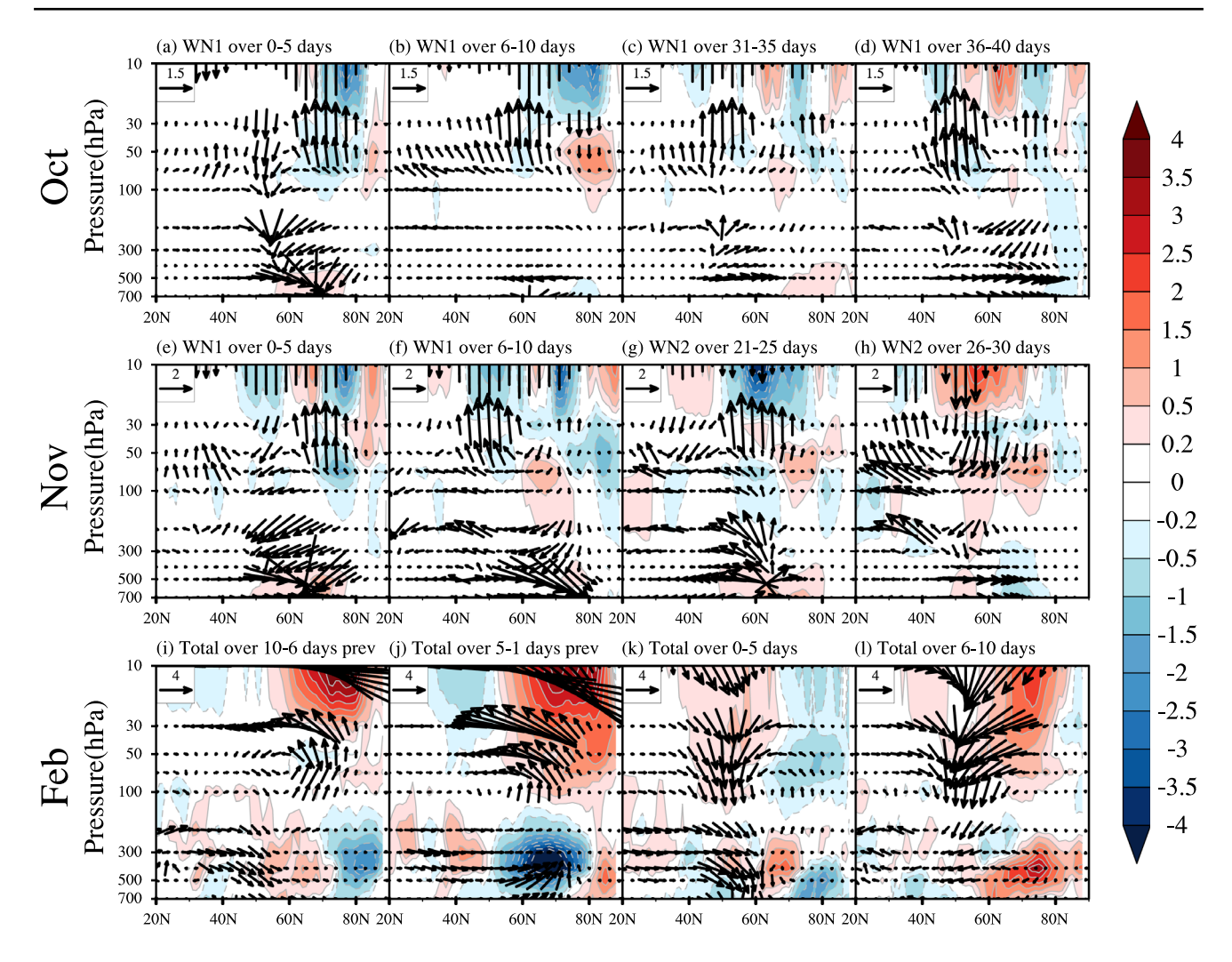


Fig. 9 Latitude–pressure cross sections of anomalous EP flux (vectors; m^2 s⁻²) and its divergence (shading; $m \cdot s^{-1} \cdot d^{-1}$) of total waves, wave-1, and wave-2 for October (**a-d**), November (**e-h**), and February (**i-l**) SPV stretching events. The meridional and vertical compo-

nents of the EP flux are divided by 10^7 and 10^5 before the composites, respectively. The EP flux is multiplied by the square root of 1000/pressure (hPa) to better demonstrate the waves in the stratosphere (above 100-hPa)

are generally opposed to those during days 21–25 (Figs. 9g, 10g). These results imply that the onset of the East Asian cold event can more likely be attributed to the inhibited upward propagation of planetary wave-2, rather than wave-1.

To summarize the mechanism behind the surface impacts of autumn SPV stretching events in both observation and simulation, we found a combination of strengthened upward-propagating wave-2 component and weakened upward-propagating wave-1 component during the early stage (days 0–15), with the wave-1 component dominating the early cold surges, consistent with the wave characteristics of Western Hemisphere pattern (Tan and Bao 2020). Whereas during the late stage, the weakened upward-propagating wave-1 (wave-2) component following October (November) SPV stretching events can amplify tropospheric ridge and trough. It should be noted that positive WAFz100 anomalies over Siberia (across

Eastern Siberia into Alaska) during days 21–30 (21–25) following October (November) SPV stretching events are dominated by enhanced upward-propagating wave-1 (wave-2) component (Figs. 6, 8, 9, and 11), which has been previously noted by studies that have highlighted the relative roles of wave-1 and wave-2 in driving stratospheric changes (e.g., Garfinkel et al. 2010; Huang et al. 2018; Martius et al. 2009; Smith et al. 2011). Furthermore, changes in upward-propagating waves at 100 hPa are preceded by that at 300 hPa before the onset of SPV stretching events, indicating that vertical upward propagation of tropospheric signals plays a critical role in impacting stratospheric variability (Polvani and Waugh 2004). It is worth noting that the simulated signals, which capture the findings in the observation in general, are more robust, benefitting from the larger size of samples.



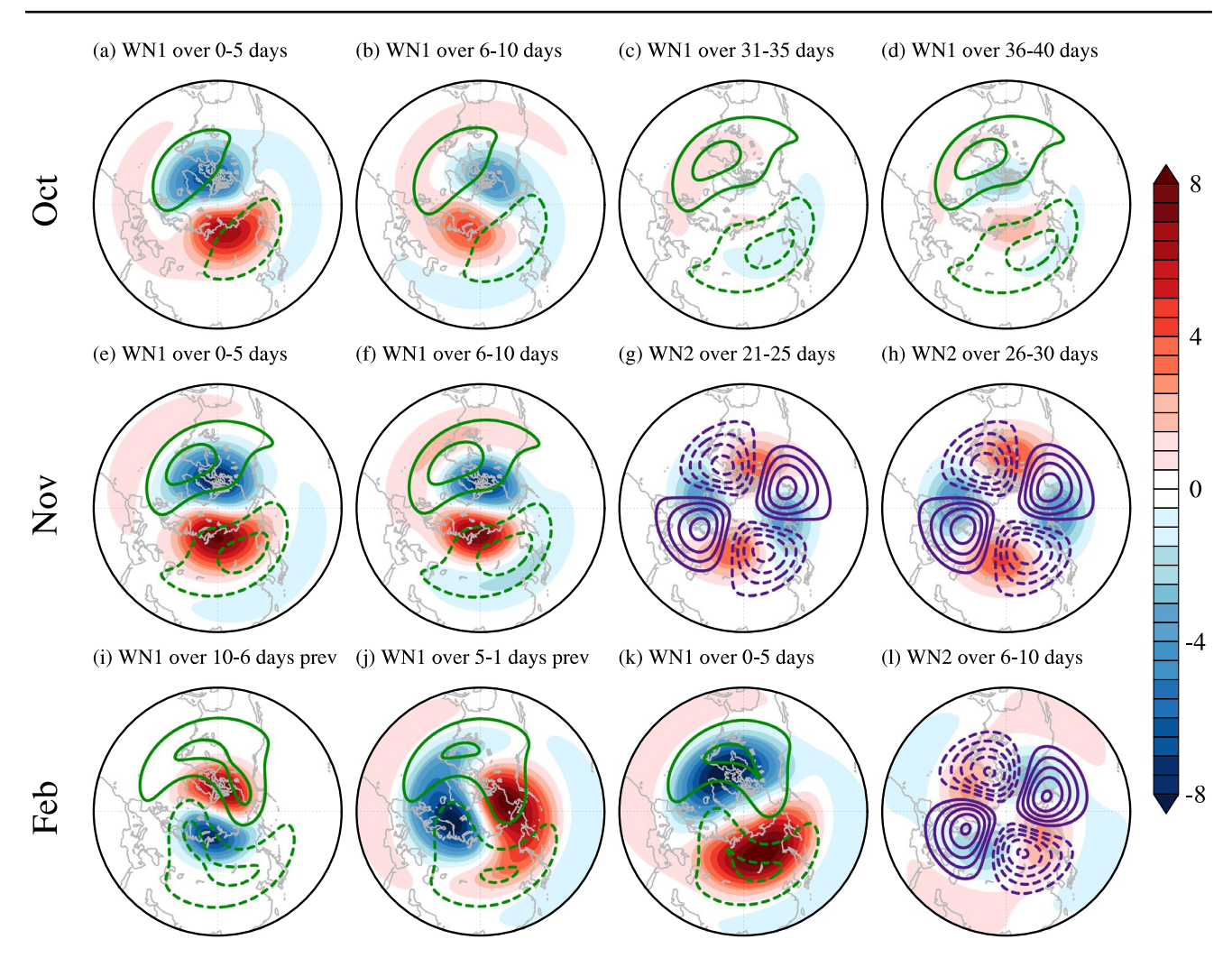


Fig. 10 The anomalous wave-1 or wave-2 height fields (color shading; units: dagpm) and corresponding climatological zonal wave-1 (green contour; contour interval is 6 dagpm) or zonal wave-2 (pur-

ple contour; contour interval is 3 dagpm) at 100-hPa in the pentad throughout the life cycles for October (**a-d**), November (**e-h**), and February (**i-l**) SPV stretching events, respectively

3.3 Mechanisms associated with late winter SPV stretching events

The relationship between late winter SPV stretching events and Eurasian SAT differs from that in autumn. Figures 4c and f show time-pressure evolutions of the normalized PCH anomalies averaged over the whole northern Eurasia for February SPV stretching events in observation and simulation. There are relatively weak and short-lived positive PCH anomalies in the troposphere centered around 500 hPa when the SPV stretching events occur during days – 4 to 8 (Fig. 4c), distinct to the features of long-lived, downward propagation from the upper stratosphere in the autumn cases (Fig. 3g–i); similarly, in simulations, the significantly positive anomalies centered within the troposphere and then extend to the surface during days – 4 to 15 (Fig. 4f). The brief and insignificantly propagating PCH anomalies from the upper stratosphere suggest that

tropospheric processes play a predominant role, rather than stratospheric processes, in influencing surface evolution following the February SPV stretching events. The corresponding evolution of tropospheric circulations shows a gradually strengthened and southward-moved Arctic-Eurasian high anomaly (Fig. 13c-g) and a wave train pattern over northern mid-high latitudes, with two vertically barotropic anomalous ridges over Europe and the Sea of Okhotsk, and one trough over Siberia (Fig. 13m-q). It is worth noting that the ridge anomalies near Europe first appear before the onset of SPV stretching events, accompanied by a collocated and significant positive anomaly of WAFz100 throughout days - 10 to 30, indicating a longer duration of anomalous upward-propagating tropospheric waves over Europe (Fig. 13k-r). The enhanced upward-propagating waves can also be found in the daily evolution of waves, particularly before the onset of SPV stretching events (Fig. 8i-l). The wave-2 configuration of 500 hPa geopotential height over



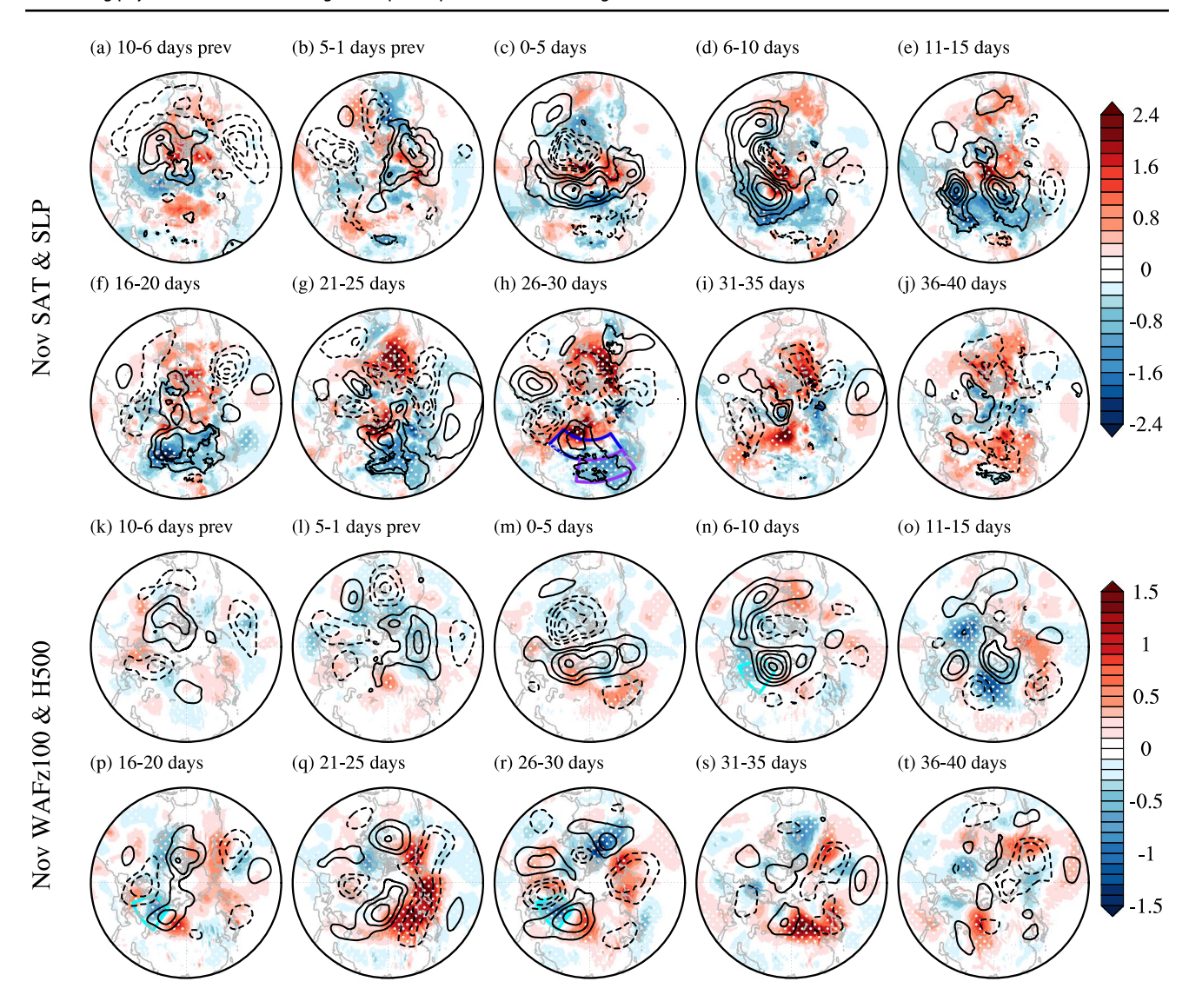


Fig. 11 As in Fig. 6, but for November SPV stretching events in observation

the high-latitudes (Fig. 13m) resembles the AkR pattern that leads to extreme cold in North America (Lee et al. 2019). The weakened upward-propagating planetary waves over Eastern Siberia-northern North Pacific during days 6-15 (Fig. 13n, o) favors the strengthening of the Eastern Siberia-Okhotsk height ridge in the troposphere, leading to significant cold anomalies over high-latitude Eurasia during days 11–25 (Fig. 13e–g). These results further indicate that the evolution of the tropospheric circulation appears to affect the stratospheric atmosphere and surface climate simultaneously, and the surface coldness is mainly triggered by European high through a tropospheric pathway rather than a long-lasting stratospheric pathway as in autumn. Similar results can be simulated in model experiments, particularly the robust surface cooling induced by the European high, although the timing of the evident cold anomalies during days 6–20 differs slightly from the observation (Fig. 14a–c). In addition, the simulated mid-tropospheric ridge anomalies are shrunk to northern Europe, corresponding to persistent upward propagation of waves as observed (Fig. 14d, e). The simulation results further demonstrate that the tropospheric pathway plays a dominant role in the surface cold surges, albeit following the onset of February SPV stretching events.

The daily evolutions of eddy heat fluxes (Fig. 8i–l) show that the strengthened or suppressed upward-propagating total waves at 100 hPa and 300 hPa emerge alternately prior to day 10: enhanced total waves during days – 7 to – 4 and weakened during days 6–7 (3–5) at 100 (300) hPa. For model experiments, the enhanced upward-propagating total waves at 100 hPa occur during days – 7 to – 6, while the weakened ones during days 2–8, generally consistent with the observations. It is well recognized that the stronger wave-1 component has more contributions to total waves before day 0, while the subsequent weaker total waves are



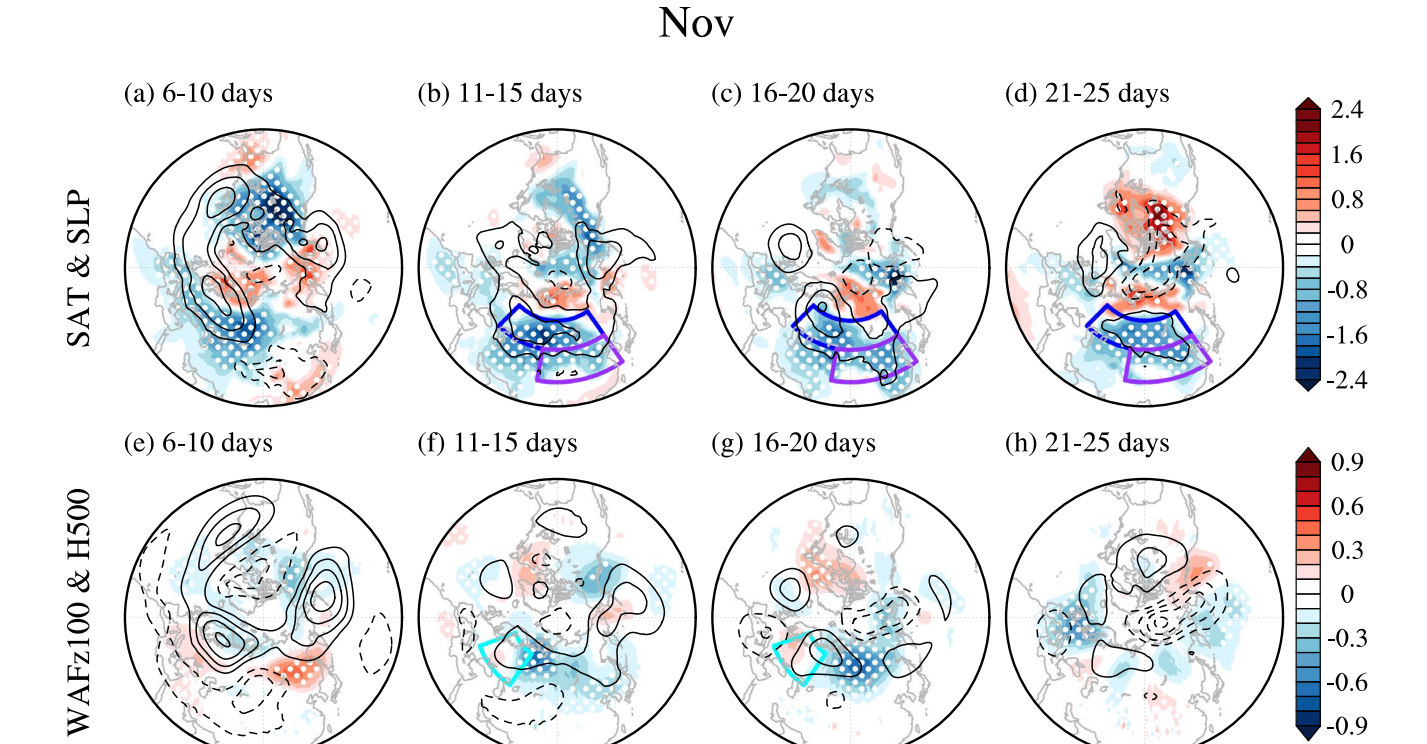


Fig. 12 As in Fig. 11, but for November SPV stretching events in the simulation. The intervals of 500-hPa geopotential height anomalies are 1 dagpm

dominantly contributed by the wave-2 component (Fig. 8i). Over the Europe region, the upward propagation of anomalous tropospheric signals before day 20 occur in two periods: one during days - 8 to 0 and the other during days 5-19 (Fig. 8k). For the first period, the European high leads to a dramatic increase in planetary waves propagating from the troposphere into the stratosphere, and thereafter, affect the SPV geometries (SPV stretching events), which is broadly consistent with strengthened total waves at 100 hPa and upward extension of PCH anomalies from mid-troposphere to lower-stratosphere (Fig. 4c, f). For the second period, the longer duration of the European high tends to enhance upward-propagating wave activity, maintaining the deep barotropic structure of the high anomaly throughout the troposphere, and result in continuous Eurasian cooling through the tropospheric pathway (Fig. 13e-g, n-p). Figure 9i-1 shows much stronger anomalies of upward (downward) propagating total waves of EP flux in the stratosphere during days -10 to -1 (days 0-10), which corresponds to the evolution of the total eddy heat flux (Fig. 8i, 1). It is obvious that the anomalous upward-propagating planetary waves over Europe are the predominant contribution of total waves that can propagate into the stratosphere, whereas the anomalously downward propagated total waves from the stratosphere to mid-troposphere are likely due to the wave activity anomalies over Okhotsk-northern North Pacific, indicating

a robust stratospheric wave reflection after the onset of SPV stretching events (Cohen et al. 2021). The 100 hPa geopotential height pattern shows constructive (destructive) interference during days – 10 to 0 (0–10), indicating that increased wave-1 (decreased wave-2) components propagate into the stratosphere (Fig. 10i–l). It indicates that the positive WAFz100 anomalies over Europe are mainly due to the constructive interference of wave-1 between the anomalous and climatological geopotential height.

Compared with the downward impacts of autumn SPV stretching events, the late winter SPV stretching events are preceded by enhanced upward propagation of tropospheric planetary waves induced by European high, and the longer duration of European high plays an initiating role in the formation of SPV stretching and Eurasian cooling. Their similarity is that the eddy heat flux anomalies of all wavenumbers are dominantly negative during the early stage of SPV stretching events due to the strong and long-lasting wave-1 components.

4 Conclusions and discussion

This work investigates the surface impacts of autumn and late winter SPV stretching on Eurasian SAT and the underlying physical mechanisms. It's important to note that this



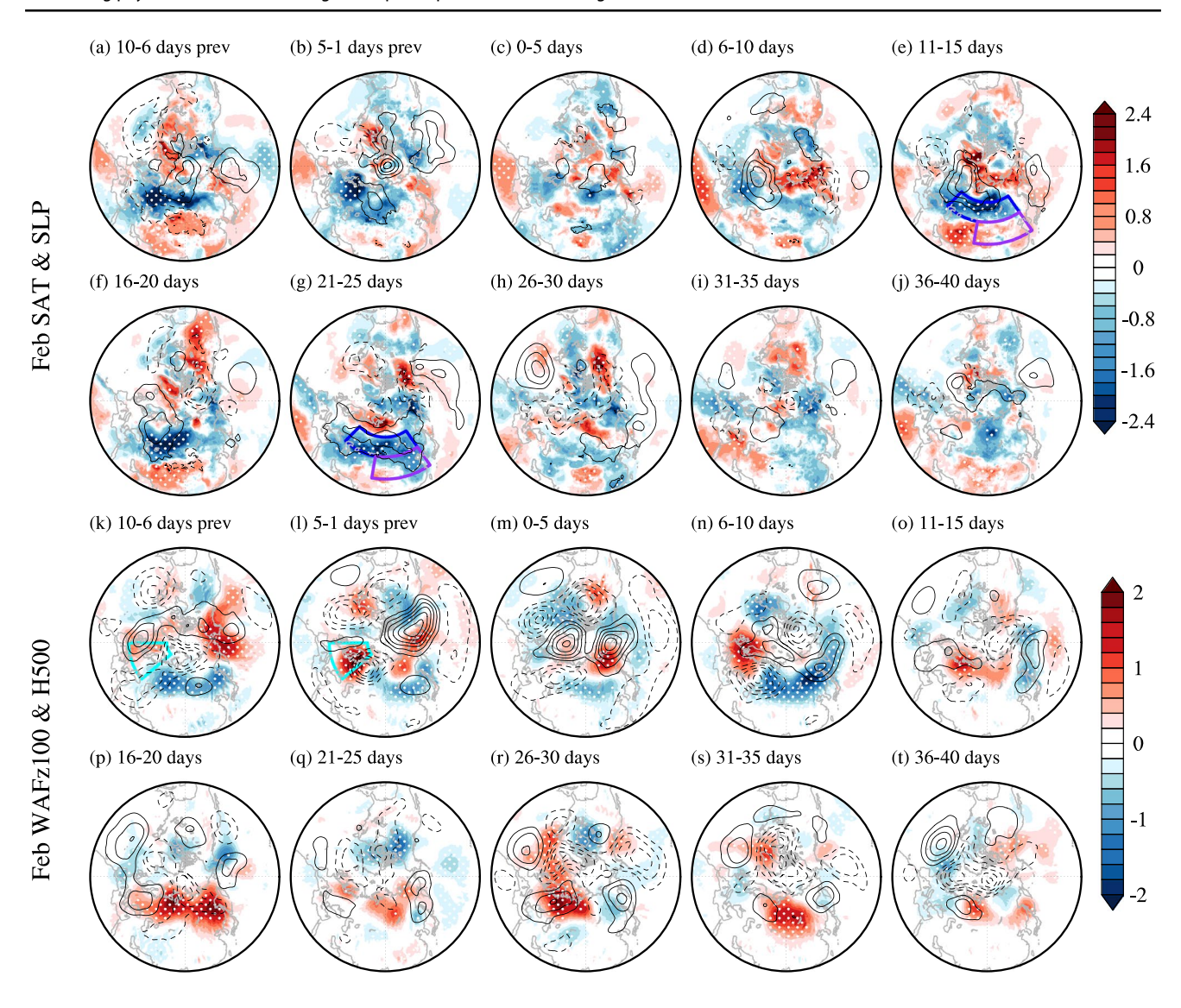


Fig. 13 As in Fig. 6, but for February SPV stretching events in observation. The intervals of SLP are 1.5 hPa. Cyan boxes in k and l highlight the key region of anomalous upward propagation of planetary waves

study seeks to delineate the distinctions in the physical mechanisms between autumn and late winter. As such, we place a strong emphasis on the qualitative significance of both tropospheric and stratospheric pathways in relation to surface cooling. For autumn SPV stretching events, the downward extension of stratospheric signals during the early stage directly results in negative AO/NAO-like anomalies and thereby the first cold anomalies in northern Eurasia. This pattern is broadly consistent with the lagged effect of the planetary wave-1 pattern (Ding et al. 2022, 2023) and the features of the Eurasia-weakened pattern notified by Liang et al. (2023). The deepening of the East Asian trough and the increase of the Ural high associated with stratospheric wave activity during the late stage are favorable for the second cold surge in high-latitude Eurasia and mid-latitude East Asia respectively. The suppressed upward-propagating

wave-1 components are responsible for the two stages of stratospheric-tropospheric wave activities and associated Eurasian cold events following the October SPV stretching events. In comparison, for the November SPV stretching events, the suppressed upward-propagating wave-1 component during the early stage contributes to the high-latitude high anomaly via a stratospheric pathway, and the suppressed upward-propagating wave-2 component during the late stage amplifies mid-latitude wave trains via a tropospheric pathway.

However, for late winter SPV stretching events, the physical mechanisms differ from that in the autumn, with a tropospheric pathway dominating the cold surface spells, as noted in previous studies that emphasized a key role of the tropospheric pathway in North American cold in February 2021 (Albers et al. 2023; Davis et al. 2022; Ding et al. 2023).



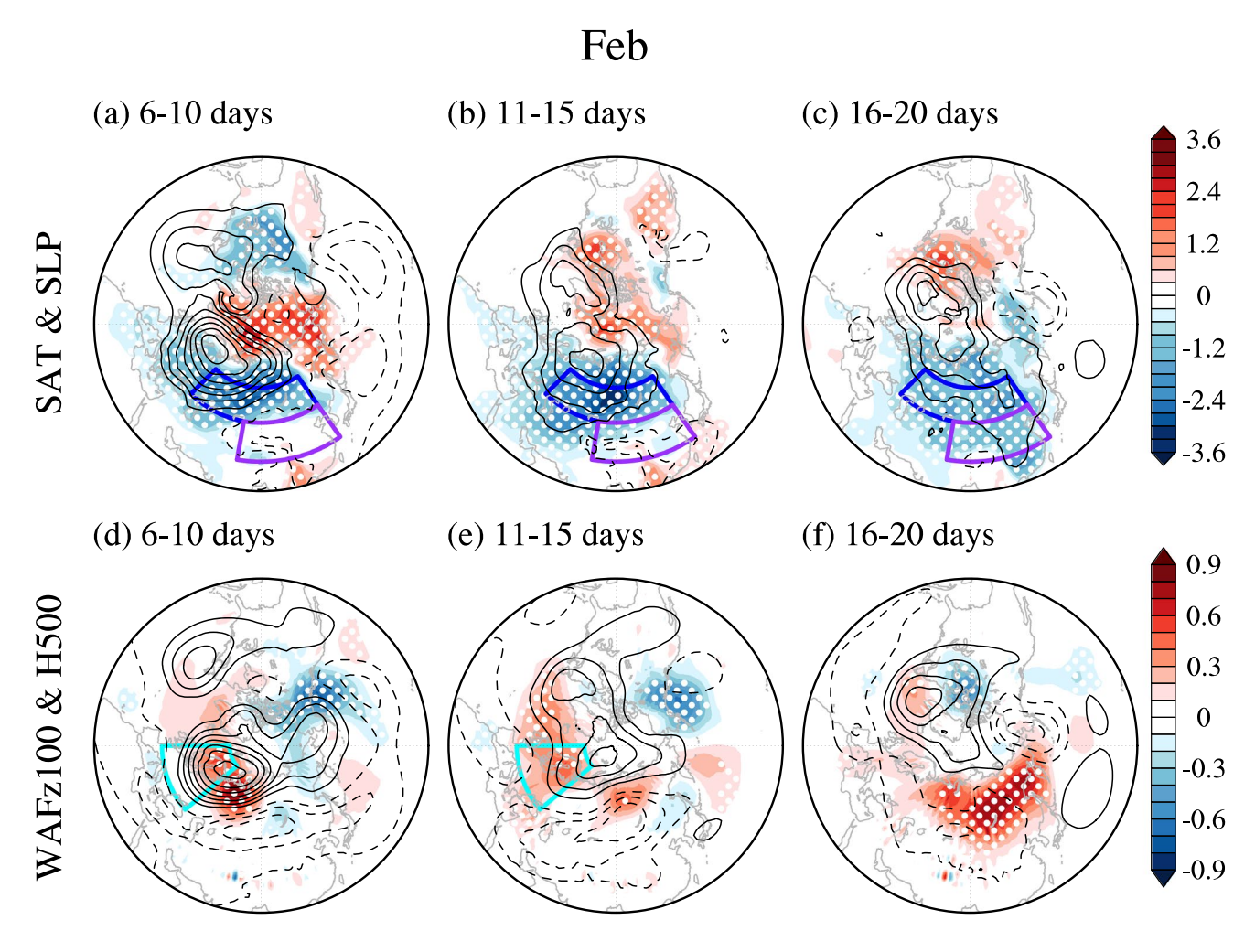


Fig. 14 As in Fig. 13, but for February SPV stretching events in the simulation. The intervals of SLP (500-hPa geopotential height anomalies) are 1 hPa (1 dagpm)

Specifically, the intensified European high acts as a possible tropospheric precursor for the February SPV stretching events, which gives rise to long-lasting and enhanced upward-propagating total waves into the stratosphere and simultaneously colder high-latitude Eurasia on the surface at sub-monthly timescales. Yu et al. (2023) have demonstrated that the sub-monthly changes of the tropospheric waves and their associated propagation are the main dynamical drivers of Eurasian CAOs, which agrees well with our results that surface cooling during February events is generally beyond the impacts of downward-propagating stratospheric signals. In summary, the tropospheric pathway, rather than the stratospheric pathway, is the primary influence on surface effects.

In the context of more frequent weak polar vortex events, our results imply contrasting mechanisms linking SPV stretching events to cold Eurasia between autumn and late winter. However, there are some caveats to this mechanism. First, separating the tropospheric and stratospheric pathways may need further parallel control runs with specific levels

of stratosphere or troposphere nudged (Ding et al. 2023; Xu et al. 2021, 2023; Zhang et al. 2018, 2020). Although we have conducted 50-sample of nudged runs (figure not shown), the size of sample may be insufficient, and further experiments with more ensemble members would be more compelling. Second, the current WACCM experiments are forced with climatological surface conditions, but a historical evolution of surface conditions can involve more realistic interannual variations. The advantage of the current run would be to avoid the interference of sea ice changes, which can exert large influence on the occurrence of SPV stretching events. Thus, further experiments with historical boundary forcings and comprehensive mechanisms would be helpful to better understand the surface impacts of stratospheric changes.

Although the temporal evolutions related to the findings in the observation are statistically significant, the limited sample size makes them somewhat noisy. The trivial signals in the observation could hinder the application of the



stratospheric precursor to sub-seasonal weather prediction. However, our simulation, which employs a well-resolved stratosphere model, demonstrates that the current model development is generally capable of simulating the downward influence of SPV stretching. Moreover, benefiting from the large sample sizes, the model simulation instills more confidence in our findings regarding the distinct role of total waves, wave-1 and wave-2 in the surface weather development accompanied by SPV stretching events.

Acknowledgements R.N.Z. was supported by the National Natural Science Foundation of China (NSFC; Grant 42288101), the National Key Research and Development Program (Grant 2022YFF0801703) and the NSFC (Grant 42075016). P.Z. is supported by NSF grant AGS-2232582.

Funding National Key Research and Development Program, 2022YFF0801703, Ruonan Zhang, National Natural Science Foundation of China, 42288101, Ruonan Zhang, 42075016, Ruonan Zhang.

Data availability The ERA5 reanalysis data from the ECWMF can be downloaded from the website: https://cds.climate.copernicus.eu.

Code availability Contact author through email.

Declarations

Conflict of interest The authors have no competing interests to declare that are relevant to the content of this article.

References

- Albers JR, Newman M, Hoell A, Breeden ML, Wang Y, Lou J (2023) The February 2021 cold air outbreak in the united states: a subseasonal forecast of opportunity. Bull Am Meteor Soc 103(12):E2887–E2904. https://doi.org/10.1175/BAMS-D-21-0266.1
- Andrews DG, Leovy CB, Holton JR (1987) Middle atmosphere dynamics, vol 40. Academic Press, New York
- Baldwin MP, Dunkerton TJ (2001) Stratospheric harbingers of anomalous weather regimes. Science 294(5542):581–584. https://doi.org/10.1126/science.1063315
- Baldwin MP, Thompson DWJ (2009) A critical comparison of stratosphere–troposphere coupling indices. Q J R Meteorol Soc 135(644):1661–1672. https://doi.org/10.1002/qj.479
- Baldwin MP, Ayarzaguena B, Birner T, Butchart N, Butler AH, Charlton-Perez AJ et al (2021) Sudden stratospheric warmings. Rev Geophys 59(1):e2020RG000708. https://doi.org/10.1029/2020RG000708
- Baldwin M, Dunkerton T (1999) Propagation of the Arctic Oscillation from the stratosphere to the troposphere. J Geophys Res Atmos 104(D24):30937–30946. https://doi.org/10.1029/1999JD900445
- Bao M, Tan X, Hartmann DL, Ceppi P (2017) Classifying the tropospheric precursor patterns of sudden stratospheric warmings. Geophys Res Lett 44(15):8011–8016. https://doi.org/10.1002/2017GL074611
- Butler AH, Seidel DJ, Hardiman SC, Butchart N, Birner T, Match A (2015) Defining sudden stratospheric warmings. Bull Am Meteorol Soc 96(11):1913–1928. https://doi.org/10.1175/BAMS-D-13-00173.1

- Butler AH, Sjoberg JP, Seidel DJ, Rosenlof KH (2017) A sudden stratospheric warming compendium. Earth Syst Sci Data 9(1):63–76. https://doi.org/10.5194/essd-9-63-2017
- Charlton AJ, Polvani LM (2007) A new look at stratospheric sudden warmings. Part I: Climatology and modeling benchmarks. J Clim 20(3):449–469. https://doi.org/10.1175/JCLI3996.1
- Cohen J, Screen JA, Furtado JC, Barlow M, Whittleston D, Coumou D et al (2014) Recent Arctic amplification and extreme midlatitude weather. Nat Geosci 7(9):627–637. https://doi.org/10.1038/ngeo2234
- Cohen J, Zhang X, Francis J, Jung T, Kwok R, Overland J et al (2020) Divergent consensuses on Arctic amplification influence on midlatitude severe winter weather. Nat Clim Chang 10(1):20–29. https://doi.org/10.1038/s41558-019-0662-y
- Cohen J, Agel L, Barlow M, Garfinkel CI, White I (2021) Linking Arctic variability and change with extreme winter weather in the United States. Science 373(6559):1116–1121. https://doi.org/10.1126/science.abi9167
- Cohen J, Agel L, Barlow M, Furtado JC, Kretschmer M, Wendt V (2022) The "Polar Vortex" Winter of 2013/2014. J Geophys Res Atmos 127(17). https://doi.org/10.1029/2022JD036493
- Davis NA, Richter JH, Glanville AA, Edwards J, LaJoie E (2022) Limited surface impacts of the January 2021 sudden stratospheric warming. Nat Commun 13(1):1–11. https://doi.org/10. 1038/s41467-022-28836-1
- Ding X, Chen G, Sun L, Zhang P (2022) Distinct North American cooling signatures following the zonally symmetric and asymmetric modes of winter stratospheric variability. Geophys Res Lett 49(6):e2021GL096076. https://doi.org/10.1029/2021GL096076
- Ding X, Chen G, Zhang P, Domeisen DIV, Orbe C (2023) Extreme stratospheric wave activity as harbingers of cold events over North America. Commun Earth Environ 4(1):187. https://doi.org/10.1038/s43247-023-00845-y
- Domeisen DIV, Butler AH (2020) Stratospheric drivers of extreme events at the Earth's surface. Commun Earth Environ 1(1):59. https://doi.org/10.1038/s43247-020-00060-z
- Domeisen DIV, Butler AH, Charlton-Perez AJ, Ayarzagüena B, Baldwin MP, Dunn-Sigouin E et al (2020) The role of the stratosphere in subseasonal to seasonal prediction: 1. Predictability of the stratosphere. J Geophys Res: Atmos 125(2):e2019JD030920. https://doi.org/10.1029/2019JD030920
- Dunn-Sigouin E, Shaw TA (2015) Comparing and contrasting extreme stratospheric events, including their coupling to the tropospheric circulation. J Geophys Res Atmos 120(4):1374–1390. https://doi.org/10.1002/2014JD022116
- Garfinkel CI, Hartmann DL, Sassi F (2010) Tropospheric precursors of anomalous Northern Hemisphere stratospheric polar vortices. J Clim 23(12):3282–3299. https://doi.org/10.1175/2010JCLI3010.1
- Garfinkel CI, Son SW, Song K, Aquila V, Oman LD (2017) Stratospheric variability contributed to and sustained the recent hiatus in Eurasian winter warming. Geophys Res Lett 44(1):374–382. https://doi.org/10.1002/2016GL072035
- Hall RJ, Mitchell DM, Seviour WJM, Wright CJ (2021) Tracking the stratosphere-to-surface impact of sudden stratospheric warmings. J Geophys Res: Atmos 126(3):e2020JD033881. https://doi.org/10. 1029/2020JD033881
- Hersbach H, Bell B, Berrisford P, Hirahara S, Horanyi A, Munoz-Sabater J et al (2020) The ERA5 global reanalysis. Q J R Meteorol Soc 146(730):1999–2049. https://doi.org/10.1002/qj.3803
- Hitchcock P, Simpson IR (2014) The downward influence of stratospheric sudden warmings. J Atmos Sci 71(10):3856–3876. https:// doi.org/10.1175/JAS-D-14-0012.1
- Huang J, Tian W (2019) Eurasian cold air outbreaks under different Arctic stratospheric polar vortex strengths. J Atmos Sci 76(5):1245–1264. https://doi.org/10.1175/JAS-D-18-0285.1



Huang J, Tian W, Gray LJ, Zhang J, Li Y, Luo J, Tian H (2018) Preconditioning of Arctic stratospheric polar vortex shift events. J Clim 31(14):5417–5436. https://doi.org/10.1175/JCLI-D-17-0695.1

- Huang J, Hitchcock P, Maycock AC, McKenna CM, Tian W (2021) Northern hemisphere cold air outbreaks are more likely to be severe during weak polar vortex conditions. Commun Earth Environ 2(1):147. https://doi.org/10.1038/s43247-021-00215-6
- Kidston J, Scaife AA, Hardiman SC, Mitchell DM, Butchart N, Baldwin MP, Gray LJ (2015) Stratospheric influence on tropospheric jet streams, storm tracks and surface weather. Nature Geosci 8(6):433–440. https://doi.org/10.1038/NGEO2424
- Kim BM, Son SW, Min SK, Jeong JH, Kim SJ, Zhang X et al (2014) Weakening of the stratospheric polar vortex by Arctic sea-ice loss. Nat Commun 5:4646. https://doi.org/10.1038/ncomms5646
- King AD, Butler AH, Jucker M, Earl NO, Rudeva I (2019) Observed relationships between sudden stratospheric warmings and European climate extremes. J Geophys Res Atmos 124(24):13943– 13961. https://doi.org/10.1029/2019JD030480
- Kodera K, Mukougawa H, Itoh S (2008) Tropospheric impact of reflected planetary waves from the stratosphere. Geophys Res Lett 35(16):L16806. https://doi.org/10.1029/2008GL034575
- Kodera K, Mukougawa H, Fujii A (2013) Influence of the vertical and zonal propagation of stratospheric planetary waves on tropospheric blockings. J Geophys Res: Atmos 118(15):8333–8345. https://doi.org/10.1002/jgrd.50650
- Kodera K, Mukougawa H, Maury P, Ueda M, Claud C (2016) Absorbing and reflecting sudden stratospheric warming events and their relationship with tropospheric circulation. J Geophys Res: Atmos 121(1):80–94. https://doi.org/10.1002/2015JD023359
- Kolstad EW, Breiteig T, Scaife AA (2010) The association between stratospheric weak polar vortex events and cold air outbreaks in the Northern Hemisphere. Q J R Meteorol Soc 136(649):886–893. https://doi.org/10.1002/qj.620
- Kretschmer M, Coumou D, Agel L, Barlow M, Tziperman E, Cohen J (2018a) More-persistent weak stratospheric polar vortex states linked to cold extremes. Bull Am Meteor Soc 99(1):49–60. https://doi.org/10.1175/BAMS-D-16-0259.1
- Kretschmer M, Cohen J, Matthias V, Runge J, Coumou D (2018b) The different stratospheric influence on cold-extremes in Eurasia and North America. Npj Clim Atmos Sci 1:44. https://doi.org/10. 1038/s41612-018-0054-4
- Lee SH, Furtado JC, Charlton-Perez AJ (2019) Wintertime North American weather regimes and the Arctic stratospheric polar vortex. Geophys Res Lett 46(24):14892–14900. https://doi.org/ 10.1029/2019GL085592
- Lehtonen I, Karpechko AY (2016) Observed and modeled tropospheric cold anomalies associated with sudden stratospheric warmings. J Geophys Res Atmos 121(4):1591–1610. https://doi.org/10.1002/2015JD023860
- Liang Z, Rao J, Guo D, Lu Q, Shi C (2023) Northern winter stratospheric polar vortex regimes and their possible influence on the extratropical troposphere. Clim Dyn 60(9–10):3167–3186. https:// doi.org/10.1007/s00382-022-06494-9
- Lu Q, Rao J, Liang Z, Guo D, Luo J, Liu S et al (2021) The sudden stratospheric warming in January 2021. Environ Res Lett 16(8):084029. https://doi.org/10.1088/1748-9326/ac12f4
- Luo D, Xiao Y, Yao Y, Dai A, Simmonds I, Franzke CLE (2016) Impact of Ural blocking on winter warm Arctic-cold Eurasian anomalies. Part I: blocking-induced amplification. J Clim 29(11):3925–3947. https://doi.org/10.1175/JCLI-D-15-0611.1
- Martius O, Polvani LM, Davies HC (2009) Blocking precursors to stratospheric sudden warming events. Geophys Res Lett 36:L14806. https://doi.org/10.1029/2009GL038776
- Matthias V, Kretschmer M (2020) The influence of stratospheric wave reflection on North American cold spell. Monthly Weather Rev 148(4):1675–1690. https://doi.org/10.1175/MWR-D-19-0339.1

- Messori G, Kretschmer M, Lee SH, Wendt V (2022) Stratospheric downward wave reflection events modulate North American weather regimes and cold spells. Weather Clim Dyn 3:1215–1236. https://doi.org/10.5194/wcd-3-1215-2022
- Mitchell DM, Charlton-Perez AJ, Gray LJ (2011) Characterizing the variability and extremes of the stratospheric polar vortices using 2D moment analysis. J Atmos Sci 68(6):1194–1213. https://doi.org/10.1175/2010JAS3555.1
- Mitchell DM, Gray LJ, Anstey J, Baldwin MP, Charlton-Perez AJ (2013) The influence of stratospheric vortex displacements and splits on surface climate. J Clim 26(8):2668–2682. https://doi.org/10.1175/JCLI-D-12-00030.1
- Nath D, Wen C, Lin W, Yin M (2014) Planetary wave reflection and its impact on tropospheric cold weather over Asia during January 2008. Adv Atmos Sci 31(4):851–862. https://doi.org/10.1007/s00376-013-3195-8
- Peings Y, Magnusdottir G (2014) Response of the wintertime Northern Hemisphere Atmospheric circulation to current and projected arctic sea ice decline: a numerical study with CAM5. J Clim 27(1):244–264. https://doi.org/10.1175/JCLI-D-13-00272.1
- Plumb R (1985) On the three-dimensional propagation of stationary waves. J Atmos Sci 42(3):217–229. https://doi.org/10.1175/1520-0469(1985)042%3c0217:OTTDPO%3e2.0.CO;2
- Polvani L, Waugh D (2004) Upward wave activity flux as a precursor to extreme stratospheric events and subsequent anomalous surface weather regimes. J Clim 17(18):3548–3554. https://doi.org/10.1175/1520-0442(2004)017%3c3548:UWAFAA%3e2.0.CO;2
- Rao J, Ren R, Chen H, Yu Y, Zhou Y (2018) The stratospheric sudden warming event in February 2018 and its prediction by a climate system model. J Geophys Res Atmos 123(23):13332–13345. https://doi.org/10.1029/2018JD028908
- Rao J, Garfinkel CI, Chen H, White IP (2019) The 2019 new year stratospheric sudden warming and its real-time predictions in multiple S2S models. J Geophys Res Atmos 124(21):11155–11174. https://doi.org/10.1029/2019JD030826
- Rao J, Garfinkel CI, White IP (2020) Predicting the downward and surface influence of the February 2018 and January 2019 sudden stratospheric warming events in subseasonal to seasonal (S2S) models. J Geophys Res: Atmos 125(2):e2019JD031919. https:// doi.org/10.1029/2019JD031919
- Scaife AA, Karpechko AY, Baldwin MP, Brookshaw A, Butler AH, Eade R et al. (2016) Seasonal winter forecasts and the stratosphere. Atmos Sci Lett 17(1):51–56. https://doi.org/10.1002/asl. 598
- Shen X, Wang L, Scaife AA, Hardiman SC, Xu P (2023) The stratosphere-troposphere oscillation as the dominant intraseasonal coupling mode between the stratosphere and troposphere. J Clim 36(7):2259–2276. https://doi.org/10.1175/JCLI-D-22-0238.1
- Sigmond M, Scinocca JF, Kharin VV, Shepherd TG (2013) Enhanced seasonal forecast skill following stratospheric sudden warmings. Nature Geosci 6(2):98–102. https://doi.org/10.1038/NGEO1698
- Smith KL, Kushner PJ (2012) Linear interference and the initiation of extratropical stratosphere–troposphere interactions. J Geophys Res: Atmos 117:D13107. https://doi.org/10.1029/2012JD017587
- Smith KL, Kushner PJ, Cohen J (2011) The role of linear interference in northern annular mode variability associated with Eurasian snow cover extent. J Clim 24(23):6185–6202. https://doi.org/10. 1175/JCLI-D-11-00055.1
- Smith KL, Neely RR, Marsh DR, Polvani LM (2014) The specified chemistry whole atmosphere community climate model (SC-WACCM). J Adv Model Earth Syst 6(3):883–901. https://doi. org/10.1002/2014MS000346
- Sun L, Deser C, Tomas RA (2015) Mechanisms of stratospheric and tropospheric circulation response to projected arctic sea ice loss. J Clim 28(19):7824–7845. https://doi.org/10.1175/ JCLI-D-15-0169.1



- Tan X, Bao M (2020) Linkage between a dominant mode in the lower stratosphere and the western hemisphere circulation pattern. Geophys Res Lett 47(17):e2020GL090105. https://doi.org/10.1029/2020GL090105
- Thompson D, Wallace J (2001) Regional climate impacts of the Northern Hemisphere annular mode. Science 293(5527):85–89. https://doi.org/10.1126/science.1058958
- Wang Y, Yasunari T (1994) A diagnostic analysis of the wave train propagating from high-latitudes to low-latitudes in early summer. J Meteorol Soc Jpn 72(2):269–279. https://doi.org/10.2151/jmsj1 965.72.2 269
- Wang L, Chen W (2010) Downward Arctic Oscillation signal associated with moderate weak stratospheric polar vortex and the cold December 2009. Geophys Res Lett 37:L09707. https://doi.org/10.1029/2010GL042659
- Waugh DW, Sobel AH, Polvani LM (2017) What is the polar vortex and how does it influence weather? Bull Am Meteor Soc 98(1):37–44. https://doi.org/10.1175/BAMS-D-15-00212.1
- White IP, Garfinkel CI, Cohen J, Jucker M, Rao J (2021) The impact of split and displacement sudden stratospheric warmings on the troposphere. J Geophys Res Atmos 126(8):e2020JD033989. https:// doi.org/10.1029/2020JD033989
- Woollings T, Charlton-Perez A, Ineson S, Marshall AG, Masato G (2010) Associations between stratospheric variability and tropospheric blocking. J Geophys Res: Atmos 115:D06108. https://doi.org/10.1029/2009JD012742
- Xie F, Ma X, Li J, Tian W, Ruan C, Sun C (2020) Using observed signals from the Arctic stratosphere and Indian ocean to predict April–May precipitation in Central China. J Clim 33(1):131–143. https://doi.org/10.1175/JCLI-D-18-0512.1
- Xu M, Tian W, Zhang J, Screen JA, Huang J, Qie K, Wang T (2021) Distinct tropospheric and stratospheric mechanisms linking historical Barents-Kara sea-ice loss and late winter Eurasian temperature variability. Geophys Res Lett 48(20):e2021GL095262. https://doi.org/10.1029/2021GL095262
- Xu Q, Chen W, Song L (2022) Two leading modes in the evolution of major sudden stratospheric warmings and their distinctive surface

- influence. Geophys Res Lett 49(2):e2021GL095431. https://doi.org/10.1029/2021GL095431
- Xu M, Tian W, Zhang J, Screen JA, Zhang C, Wang Z (2023) Important role of stratosphere–troposphere coupling in the Arctic mid-toupper tropospheric warming in response to sea-ice loss. Npj Clim Atmos Sci 6(1):9. https://doi.org/10.1038/s41612-023-00333-2
- Yang XY, Yuan X, Ting M (2016) Dynamical link between the barentskara sea ice and the arctic oscillation. J Clim 29(14):5103–5122. https://doi.org/10.1175/JCLI-D-15-0669.1
- Yu Y, Ren R, Liu B, Wang L, Chen H, Yang Y (2023) When and how can the stratosphere modify the midlatitude cold air outbreaks in northern winter: an isentropic meridional mass circulation view. J Geophys Res: Atmos 128(16):e2023JD038601. https://doi.org/ 10.1029/2023JD038601
- Zhang P, Wu Y, Simpson IR, Smith KL, Zhang X, De B, Callaghan P (2018) A stratospheric pathway linking a colder Siberia to Barents-Kara Sea sea ice loss. Sci Adv 4(7):eaat6025. https://doi.org/10.1126/scjadv.aat6025
- Zhang P, Wu Y, Chen G, Yu Y (2020) North American cold events following sudden stratospheric warming in the presence of low Barents-Kara Sea sea ice. Environ Res Lett 15(12):124017. https://doi.org/10.1088/1748-9326/abc215
- Zhang R, Screen JA, Zhang R (2022) Arctic and Pacific ocean conditions were favorable for cold extremes over Eurasia and North America during winter 2020/21. Bull Am Meteor Soc 103(10):E2285–E2301. https://doi.org/10.1175/BAMS-D-21-0264.1

Publisher's Note Springer Nature remains neutral with regard to jurisdictional claims in published maps and institutional affiliations.

Springer Nature or its licensor (e.g. a society or other partner) holds exclusive rights to this article under a publishing agreement with the author(s) or other rightsholder(s); author self-archiving of the accepted manuscript version of this article is solely governed by the terms of such publishing agreement and applicable law.

